This is a preprint, the final version is subject to change, of the American Mineralogist (MSA)
Cite as Authors (Year) Title. American Mineralogist, in press.
DOI: https://doi.org/10.2138/am-2018-6477

Revision-1

Sulfide partial melting and chalcopyrite disease: an experimental study

Boddepalli Govindarao, Kamal Lochan Pruseth and Biswajit Mishra

Department of Geology and Geophysics, Indian Institute of Technology

Kharagpur – 721302, INDIA

ABSTRACT

Speckling of sphalerite with micrometer sized blebs of chalcopyrite is usually referred to as "chalcopyrite disease". Fe-rich sphalerites are particularly prone to chalcopyrite disease. Considering the low degree of solid solution between sphalerite and chalcopyrite, exsolution is discarded as a process to explain the development of chalcopyrite disease. Diffusion-controlled replacement of Fe by Cu, and sphalerite-chalcopyrite co-precipitation rather are invoked as the most probable mechanisms. Although metamorphism is expected to dispel inhomogeneities through recrystallization, chalcopyrite disease interestingly appears unaffected and be quite common in metamorphosed sulfide ores. . We have conducted experiments on different bulk compositions in the system ZnS-PbS-FeS-Cu_2S-As_2S_3 at 600 °C and annealed the run products containing melt at 350 °C to evaluate the role of sulfide partial melting, if any, in the development of chalcopyrite disease. The results indicate that chalcopyrite blebs developed only in those sphalerites that contained Fe and in which S atoms were in excess over Fe + Zn atoms. Also it was observed that the occurrence of Fe-bearing sphalerite and the sulfide partial melt (that invariably was S-deficient and Cu-enriched) in direct contact with each other was necessary for the chalcopyrite blebs to form. We propose nonstoichiometry driven diffusion of Cu as the mechanism and sulfide partial melting as the principal causative factor behind the development of chalcopyrite disease in sphalerite.

Chalcopyrite disease thus may be used as an easily identifiable potential indicator of sulfide partial melting in metamorphosed base metal sulfide deposits.

Keywords: chalcopyrite disease, chalcopyrite blebs, sulfide partial melting, nonstoichiometry, sphalerite.

INTRODUCTION

Chalcopyrite disease is a texture that is locally found in sphalerite in which unevenly distributed, variably sized blebs of chalcopyrite occur throughout a grain of sphalerite (Fig.1). The term "chalcopyrite disease" was first introduced by Barton (1978) while describing the sphalerite textures from the Furutobe Mine, Akita Prefecture, Japan. On the basis of size of the chalcopyrite blebs and their distribution patterns Barton and Bethke (1987) further categorized the disease textures as watermelon, dusting and bimodal types. The chalcopyrite disease texture is commonly observed in natural ores from various types of deposits such as Zn- and Cu-bearing hydrothermal veins, volcanogenic and metamorphosed massive sulfide deposits (Barton and Skinner, 1967). The origin of the chalcopyrite disease texture in sphalerite has been a topic of debate for several years. Unmixing of chalcopyrite from a high-temperature sphalerite solid solution has been discarded on the basis of results of several experimental studies in the Cu-Fe-Zn-S system (Wiggins and Craig, 1980; Hutchison and Scott, 1981; Kojima and Sugaki, 1984, 1985) showing that the solubility of Cu in sphalerite is disproportionately low compared to the amount of chalcopyrite observed in the diseased sphalerites. Bulk compositions of most of the diseased natural sphalerites fall outside the Cu-solubility range even at 800°C, when plotted in the CuS-FeS-ZnS system and suggest that exsolution is unlikely to produce chalcopyrite blebs from sphalerite (Sugaki et al., 1987; Barton and Bethke, 1987). The replacement of Fe by Cu in Fe-rich sphalerites has been alternatively proposed to have produced chalcopyrite disease (Barton, 1978; Barton and

Bethke, 1987), which is supported by the experimental reproduction of chalcopyrite disease by reacting Fe-bearing natural sphalerites with Cu-bearing fluids (Kojima and Sugaki, 1987; Eldridge et al., 1988). In these experiments, no chalcopyrite disease developed in the Fe-poor natural sphalerites. Other mechanisms proposed for the generation of chalcopyrite disease include selective dissolution of Fe-rich sphalerite and addition of Cu or both Cu and Fe from fluid sources (Bortnikov et al., 1991) and sphalerite-chalcopyrite co-precipitation (Kojima, 1990; Kojima et al., 1995). The latter workers were successful in experimentally reproducing chalcopyrite disease in both Fe-poor and Fe-rich synthetic sphalerites. However, detailed solid-state experiments at different temperatures (400–750 °C) for variable durations, using both Fe-poor and Fe-rich sphalerites and different Cu-sulfide sources (Bente and Doering, 1993, 1995), demonstrate that disease textures develop only in Fe-rich sphalerites.

The presence of chalcopyrite disease in sphalerites from metamorphosed massive sulfide deposits is also a common observation. Sometimes the chalcopyrite-sphalerite intergrowth is so intense that it is difficult to distinguish whether sphalerite is diseased with chalcopyrite or it is the other way around (e.g., see Fig. 1B). Such intense intergrowth is definitely not a result of exsolution, considering the limited sphalerite-chalcopyrite solid solubility. No process associated with metamorphism of sulfide mineral assemblages has yet been recognized that produces chalcopyrite disease, and the occurrence of chalcopyrite-diseased sphalerite in metamorphosed ores has been ascribed only to the recrystallization of already diseased sphalerites (Scott, 1983). However, recrystallization at high temperatures may remobilize chalcopyrite inclusions within sphalerite explaining the scarcity of chalcopyrite disease in sphalerites subjected to upper amphibolite or granulite facies metamorphism (Lockington et al., 2014). Pure sphalerite is refractory (melts at 1718 °C; Sharma and Chang, 1996), and may survive even the highest grades of metamorphism. Sulfide partial melting is being growingly reported from metamorphosed ore deposits (e.g.

Mavrogenes et al., 2001; Frost et al., 2002, 2011; Tomkins and Mavrogenes, 2002, 2003, 2007; Sparks and Mavrogenes, 2005; Mishra and Bernhardt, 2009; Pruseth et al., 2014, 2016) and it is noted that sulfide partial melts are preferentially enriched in Cu (Pruseth et al., 2014, 2016). . Thus sulfide partial melting may erase chalcopyrite disease textures by causing remobilization of Cu. However, chalcopyrite disease development could be a sub-solidus process and may redevelop during cooling after partial melting. In this study, we have produced chalcopyrite disease in sphalerite, by annealing at 350 °C synthetic phase assemblages in the system ZnS-PbS-FeS-Cu_2S-As_2S_3 containing sulfide melts produced at 600 °C. The results indicate that partial melting plays a vital role in the development of chalcopyrite disease textures by promoting S-enrichment in sphalerite concomitant with the nonstoichiometric incorporation of Fe, together with the production of Cu-enriched but S-deficient sulfide melts.

EXPERIMENTAL AND ANALYTICAL METHODS

Experiments including the synthesis of the end-members were conducted by the evacuated silica tube method as described by Scott (1974) and Pruseth et al. (1997). Quartz tubes of 6 mm internal diameter and 1 mm wall thickness were used. The experimental charge is confined to the lower 0.5 cm of approximately 3 cm long evacuated quartz capsules, the upper part of which is occupied by a snugly fitting filler quartz rod. Samples were heated in a horizontal LENTON (UK) furnace with inbuilt EUROTHERM temperature controllers and the temperature in the hot zone of the furnace was externally monitored by a Pt–Pt_{90}-Rh_{10} thermocouple. The temperature in the hot zone of the furnace was maintained within ± 2 °C of the set temperature.

High purity elemental Fe, Zn, Pb, Cu and S from Alfa Aesar were used for synthesizing the sulfide end-members (FeS, ZnS, PbS, and Cu_2S). For synthesis of FeS, the

iron powder was reduced in a hydrogen flow at 800 °C for four hours followed by reacting required amount of iron and sulfur at 400 °C for four days and at 600 °C for five days. PbS was synthesized from pieces of pure Pb, cut from a sheet after removing the thin oxidized coating, which were reacted with sulfur at 500 °C for eight days. Zinc ingots were abraded to a fine powder and reacted with sulfur at 400 °C for two days and at 500 °C for five days for synthesizing ZnS. Fine copper filings, washed with dilute HCl and then with distilled water, were reacted with sulfur initially at 200 °C for two days and finally at 400 °C for nine days. Pure crystalline As_2S_3 procured from Alfa Aesar was directly used as the source of As. Accurately weighed amounts of ZnS, FeS, PbS, Cu_2S and As_2S_3 constituting five different bulk proportions were heated at 600 °C for 10 days. The relative proportions of the end-members were chosen such that in different bulk compositions total metals and S were in 1:1 atomic ratios. A small part of each of the run products was kept for microscopic characterization and chemical analysis by an electron probe micro-analyzer (EPMA) and the rest was annealed for 18 days at 350 °C in evacuated silica tubes.

Epoxy-mounted polished samples of the run products were analyzed with a CAMECA SX100 EPMA at the Department of Geology and Geophysics, IIT, Kharagpur. The typical operating conditions were 20 kV accelerating voltage, 20 nA beam current and 1μm beam diameter. The sulfide partial melt, which quenched to a fine intergrowth of different solid phases, was analyzed with a beam diameter of 20 μm under similar conditions. Several spot analyses were averaged for obtaining the closest possible composition representing the melt. The X-ray lines used for the analysis of S, Fe, Cu, Zn, As and Pb are SKα, FeKα, CuKα, ZnKα, AsLα and PbMα, respectively. Natural mineral standards of pyrite was used for the calibration of Fe and S, sphalerite for Zn, galena for Pb, GaAs for As and pure Cu metal for Cu. All standards were from the P & H Developments Ltd. (U.K.).

Backscattered electron (BSE) images were collected by using a JEOL JSM6490 scanning electron microscope (SEM).

RESULTS

Partial melting was encountered in all the five experimental runs (G18–G22). The maximum amount of melt was produced in the run products G19 and G20. The melt and bulk run compositions are plotted in Figures 2A and 2B and the experimental details and phases obtained in different run products are summarized in Table 1. Attainment of equilibrium was confirmed from the consistency of phase assemblages in experimental runs of different durations and the intra-grain and inter-grain homogeneity of compositions of the different solid phases. Selected repeat runs yielded reproducible assemblages. Melting is confirmed from the quench textures and the presence of stable newly formed euhedral and skeletal crystals of löllingite and arsenopyrite crystallizing in the melt phase, as observed in the SEM BSE images (e.g., Fig. 3). Galena, sphalerite and melt are common to all the run products. In addition, intermediate solid solution (Iss) is obtained in G18 and Iss + pyrrhotite in G22. Löllingite is stable in G19 and in G21 in which it coexists with a phase with composition close to that of koutekite (Cu_2As). Arsenopyrite is a stable phase in G20. Various phases crystallized out from the melt during quenching. Arsenopyrite and Iss are observed in the quenched melt in the case of G18 and G22 and chalcopyrite in G19 and G20. When present in the quenched melt, chalcopyrite preferentially is seen to nucleate on sphalerite grains those are in contact with the melt. A bimodality in the melt compositions is noticeable, the FeS-rich bulk compositions (G18, G22) yielding FeS-rich melts (average at% S = 41.8, Fe = 21.6, Cu = 3.7, Zn = 0.6, As = 25.0, Pb = 7.3) that are markedly enriched in As compared to the Cu-rich melts (average at% S = 46.3, Fe = 3.6, Cu = 23.4, Zn = 1.9, As = 10.7, Pb = 14.1) obtained from the FeS-poor bulk compositions (G19, G20). The melt in G21, which is

extremely FeS-poor, is enriched in Cu but very much depleted in As (at% S = 37.5, Fe = 1.4, Cu = 47.3, Zn = 1.2, As = 1.3, Pb = 11.3). However, from Figure 3 the presence of two immiscible melts is evident. These melts could not be separately analyzed as they are intimately intergrown and the unmixing of phases in each of them during quenching gave rise to further complexity. This is consistent with the observation of liquid immiscibility in experimental runs incorporating sulfosalts (Mavrogenes et al., 2013). In As-free systems, Fe-enriched melts comparable to those from G18 and G22 have been reported only above 850 °C (Stevens et al., 2005) as noted by Pruseth et al. (2014). The FeS-poor melts except the one from G21 are also significantly enriched in As. The stabilization of Cu_2As results in an As-poor melt in this case. In the absence of As, cubanite is a stable phase that governs the stabilization of a melt phase for the FeS-rich bulk compositions (Pruseth et al., 2014).

Significant nonstoichiometry is observed in galena, melt, sphalerite and Iss, depending on the initial bulk composition and the stable phase assemblage in the run products. While sphalerite and Iss are always S-enriched, melt is always S-deficient, and galena in some run products is S-enriched and in others S-deficient (Fig. 4). In G21 both galena and melt are predominantly S-deficient and sphalerite is slightly S-enriched. However, due to the ZnS-rich bulk composition, sphalerite is the most abundant phase and in spite of its not so significant S-enrichment, compensates for the S-deficiency in galena and melt. For a similar run composition but without As, Jehan (2015) and Pruseth et al. (2016) observed the presence of metallic Cu as a stable phase, which is consistent with the Cu_2As-phase obtained in the present study because of the presence of As. The degree of nonstoichiometry in sphalerite has a direct correlation with its Fe-content. The Fe-content in sphalerite varies from ~0.5 at% to as high as ~16 at%, the most Fe-rich sphalerites coming from the experimental runs with the highest FeS in their bulk. In addition to Fe, small amounts of Cu, varying in the range of 0.5–0.9 at%, are incorporated in sphalerite.

The phases obtained after annealing at 350 °C and their EPMA analyses are provided in Table 2. The ranges of nonstoichiometry in sphalerite, galena and Iss can be seen from Figure 4. The quenched melts in different run products recrystallized giving different phases depending upon their compositions. In the FeS-poor runs (G19 and G20), which produced the maximum amounts of melts, no significant change in the quenched melt texture except slight coarsening of the blebs is observed (Figs. 3B, 3D). Loss of Cu and relative gain of Fe compared to the original melt compositions is evident from the EPM analyses (Table 2). Coarsening of blebs of galena within the quenched melt of G19 (Fig. 3B) and nucleation of fresh galena blebs on pre-existing galena in G20 (Fig. 3D) are evident. Nucleation of chalcopyrite occurred on sphalerite and chalcopyrite disease developed in it (Fig. 3D). Although very fine blebs of chalcopyrite in the sphalerite of G19 can be seen through optical microscopy, they are not distinguishable in the BSE images because of very similar average atomic numbers of sphalerite and chalcopyrite. Because of the larger size and higher abundance of chalcopyrite blebs, a brighter outer zone is seen in the sphalerites in G20 (Fig. 3D). In the FeS-rich runs (G18, G22), in which Iss was a stable phase, the melt recrystallized to arsenopyrite + galena (e.g., Fig.3F) and the Iss became enriched in Cu. In the extremely FeS-poor run G21, the melt that was originally Cu- and Pb-rich, recrystallized to chalcocite ($Cu_{2.19}S$) and galena (Fig.3H).

The development of chalcopyrite disease in the outer zones of the sphalerite grains can be seen in the photomicrograph of the experimental run products (e.g., Fig. 5A). The BSE images are however not representative. The chalcopyrite-diseased outer zones in sphalerite appear only relatively brighter in the BSE images. As can be seen from Figure 5B and Table 3, the Zn-content in the diseased zone does not greatly deviate from the undiseased zone. However, Fe decreases and Cu increases from the original concentration levels attaining similar values in the diseased part. The Cu-content increases from 0.5 at% in the undiseased

core to 5.66 at% in the diseased rim, and the Fe-content decreases from 11.26 at% in the core to 6.68 at% in the rim. Sulfur, similar to Zn does not significantly vary from the undiseased to the diseased zone (Fig. 6). The nucleation of chalcopyrite at the melt-sphalerite interface and the higher density of chalcopyrite near it within the diseased zone of sphalerite are evident from the photomicrograph (Fig. 5A) as well as from the X-ray Cu map (Fig. 6A). The nucleation of a Fe-rich mineral (probably pyrrhotite) along with chalcopyrite along the sphalerite boundary is evident in Figure 6B.

DISCUSSION

Experimental data reveal that chalcopyrite disease in sphalerite cannot be a result of subsolidus exsolution as Cu is not sufficiently soluble in sphalerite, even at 800 °C, to account for the high proportions of chalcopyrite observed in the diseased portions of sphalerite (Sugaki et al., 1987; Barton and Bethke, 1987). Although a crystallographic control on the distribution of chalcopyrite blebs within sphalerite is observed (e.g., Fig. 1), such relations are incomprehensible when the blebs are coarsened and probably coalesce to impart the appearance of an intimate intergrowth-like texture generally observed when two phases simultaneously crystallize from a eutectic melt. A similar mechanism, involving coprecipitation of chalcopyrite and sphalerite has been suggested for the origin of chalcopyrite disease (Kojima, 1990; Kojima et al., 1995). The lower solubility of Cu in sphalerite warrants that for the development of chalcopyrite disease, Cu (and probably both Cu and Fe) need to be externally supplied. In fact, natural observations as well as experimental studies have confirmed that chalcopyrite disease develops only in sphalerites those are originally enriched in Fe (Barton and Bethke, 1987; Kojima and Sugaki, 1987; Eldridge et al., 1988; Bente and Doering, 1993, 1995) indicating that diffusion of Cu into sphalerite is the mechanism giving rise to chalcopyrite disease. A comparison of

compositions of the chalcopyrite-free cores of the diseased sphalerites in the present study (Tables 1, 2) reveals that the Fe-content does not appreciably change due to the annealing of the 600 °C run products at 350 °C, supporting the diffusion of Cu as the cause of chalcopyrite disease. Probably there is a limiting amount of Fe in sphalerite that is essential for initiating the diffusion of Cu into it. Bente and Doering (1993) propose a minimum Fe-content of 2–3 at% (~4–6 mol% FeS), whereas Lepetit et al. (2003) propose a minimum of 7 mol% FeS. In this study, for the experimental run G21 in which the FeS-content in sphalerite is ~1 mol%, no chalcopyrite disease developed. Some minimum amount of Cu (~0.5–1 at%) also seems to be accommodated in the structure of sphalerite without causing segregation of chalcopyrite.

Although diffusion of Cu is apparently the cause behind the development of chalcopyrite disease, the driving force for this diffusion is not well-understood and the role of diffusion itself has been questioned. For example, in a zoned natural sphalerites reported by Barton and Bethke (1987), chalcopyrite disease uniformly occupied only the Fe-rich zones without showing any gradational variation from Fe-rich to Fe-poor zones. Barton and Bethke (1987) noted that if diffusion was the mechanism, chalcopyrite blebs should have preferentially been concentrated in the compositionally steep interfaces where lattice strains might be focussed and favored diffusion. Bente and Doering (1993) ascribe chemical-potential differences between sphalerite and Cu-rich phases such as chalcopyrite, Iss, digenite and bornite, used in their experiments to be the driving force behind the origin of chalcopyrite disease or the diffusion-induced segregations (DIC), as they prefer to call it. The relative decrease of Fe in the diseased sphalerite zones was presumed by them to be due to reverse diffusion of Fe out of sphalerite. However, no gradational increase of Fe towards the outer rim of the diseased sphalerite zones is observed in this study (e.g., Fig. 6C) thereby indicating no diffusing of Fe out of sphalerite and the observed apparent decrease in Fe to be due to the

relative increase of Cu. The apparent constancy of the Zn-content may be due to the very small change on its relative proportion brought about by the addition of Cu. The higher density of chalcopyrite at the interface between the quenched melt phase and sphalerite clearly indicates that diffusion of Cu is the mechanism by which chalcopyrite disease texture forms. Differences in Fe-concentrations between the zones in zoned sphalerites, particularly when the Fe in the Fe-poor zone is lower than the threshold concentration required for chalcopyrite disease to develop, thus cannot be the driving force for the diffusion of Cu. Apparently diffusion within the Fe-rich zones takes place until a homogeneous distribution of chalcopyrite blebs is achieved. It is also possible that Fe-enriched centers scattered within Fe-rich sphalerites are the sites where chalcopyrite blebs form. Scott and Barnes (1971) have reported about the formation of Fe-enriched patches in Fe-rich sphalerites in their experiments. They postulated that formation of such Fe-rich patches may be due to preferential inclusion of FeS along certain crystal faces during the growth of sphalerite or due to retention of metastable high-T (>525 °C) polymorph/polytype of sphalerite during cooling. Chalcopyrite disease textures with exsolution-like features most likely are due to Fe-rich patches formed due to the latter process, which are later converted to chalcopyrite by the incorporation of Cu.

In the present study, chalcopyrite disease developed only in the sphalerite grains those were Fe-enriched and were in contact with melt. Sphalerite grains entirely surrounded by solid phases and thus effectively isolated from melt were not affected. It is also noteworthy that the Fe-enriched sphalerites are nonstoichiometric and contain excess S over Σmetal. As evident from Figure 4 and Table 1, the more the sphalerite is enriched in Fe the more is the degree of nonstoichiometry (see Fig. 7) in it and the higher is its S excess. Initial increase in the Fe-content up to ~5 at% does not cause any nonstoichiometry. However, beyond this concentration nonstoichiometry markedly increases with further increase of Fe. In spite of

the high nonstoichiometry of sphalerites in G18 and G22 no chalcopyrite disease developed in them because the melts produced in these runs are Cu-poor due to the stabilization of Iss and the sequestration of Cu in it. Thus, highly Fe-rich bulk compositions also may not be conducive to the formation of chalcopyrite disease, depending upon the exact nature of the stable phase assemblages produced. Sphalerites with similar excess of S, caused probably due to sulfide partial melting, have been reported from Rajpura-Dariba, India (Pruseth et al., 2014). This nonstoichiometry most likely is the driving force that causes chalcopyrite disease. However, the availability of an external source of Cu should be present, the condition that is fulfilled here by the sulfide partial melt, which is generally, in addition to being enriched in Cu, is always deficient in S relative to Σmetal. The incorporation of Fe in sphalerite takes place by the replacement of Zn depending upon the activity of Fe as well as the fugacity of S at the time of sphalerite crystallization (Barton and Skinner, 1967). However, the presence of excess S indicates the presence of cation vacancy sites suggesting the incorporation of Fe in sphalerite as a pyrrhotite component. Electrical measurements show that cation (e.g., Zn) vacancies are favored in sphalerite whereas S-vacancies are prevalent in wurtzite (Morehead, 1963). The substitution energy for the replacement of Zn-vacancy by Cu is –594.22 kJ/mol whereas that for the formation of Zn-vacancy is –110.96 kJ/mol (Chen et al., 2010) indicating the favorability of Cu-diffusion into sphalerite, once Zn-vacancies are created. Whether Cu can preferably diffuse as Cu^{+} ions or as Cu^{2+} ions is however not clear. Two unit-cells of sphalerite joined end-to-end give a unit-cell similar to that of chalcopyrite. Therefore, diffusion of Cu into Fe-enriched non-stoichiometric sphalerite may produce chalcopyrite blebs giving rise to chalcopyrite disease. The role of a favourable crystal structure is underscored by the observation that despite marked nonstoichiometry, chalcopyrite disease does not develop in pyrrhotite. In the process of chalcopyrite disease formation in sphalerite, charge imbalances are locally resolved and the invasion by Cu may continue further.

Probably scattered Fe-rich centers present in sphalerite (Scott and Barnes, 1971), having been nonstoichiometric, give rise to charge imbalance that promotes diffusion of Cu. Although Cu and Fe may exist in chalcopyrite as Cu^{+} and Fe^{3+} ions or as Cu^{2+} and Fe^{2+} ions or a mixture thereof, the question of oxidation states of Cu and Fe in chalcopyrite continues to be a matter of debate (see Pearce et al., 2006 and references therein). Pearce et al. (2006) have argued in favour of the former, but complications exist due to marked covalency (Klekovkina et al., 2014). However, the presence of As may give rise to oxidation-reduction reactions in sulfide systems as revealed by the partial reduction of pyrite to Fe-metal when reacted with As_2S_3–melt (Pruseth and Sahu, 2017). We notice also the oxidation of Fe to Fe^{3+} (unpublished work) when As_2S_3 reacts with pyrite or pyrrhotite. Thus, cation vacancy in sphalerite inferred in the present study may be due to the incorporation in it of Fe as Fe^{3+} ions and the incursion of sphalerite by chalcopyrite is not as much due to the concentration gradient in Cu or Fe as due to the availability of vacancy in cation sites. This is corroborated by the fact that chalcopyrite disease does not develop in Fe-poor sphalerites that are unlikely to contain significant concentrations of vacancy. This is due to the possibility of excess S in sphalerites consistent with the observation of the increasing nonstoichiometry in sphalerite with increasing concentrations of both Fe and S in our experiments. The nonstoichiometric excess of S-content is representative of the concentration of vacancy and is positively correlated with the Fe-content in sphalerite (Table 1 and Fig. 7). Barton and Toulmin (1966) have shown that there is a probability of incorporating excess S in Fe-rich sphalerites, as revealed from the increase of unit-cell edges in Fe-rich sphalerites when equilibrated at higher S partial pressure.

Metamorphism-induced partial melting of sulfide ores facilitates the formation of chalcopyrite disease by producing a Cu-enriched but S-deficient melt phase and Fe- and S-enriched sphalerite. There is a tendency during cooling to re-establish stoichiometry by the

diffusion of excess Cu from the solidified melt phase into sphalerite. However, for chalcopyrite disease to develop, the Cu-enriched solidified melt must exist in close contact with the Fe-enriched sphalerite, a condition that may not always be satisfied. Sulfide partial melts may migrate away from the sphalerites. Under such circumstances the Fe-enriched sphalerites may not develop any chalcopyrite disease and may produce pyrrhotite ± pyrite inclusions on reequilibration, depending upon the ambient S-fugacity. Sulfide partial melting may be a prerequisite for the production of a suitable Cu-source but nonstoichiometric Fe-bearing sphalerite may be produced by increased S-fugacity during prograde metamorphism even in the absence of partial melting. Pyrrhotite and pyrite may crystallize out from such sphalerites unless Cu-enriched mineral phases are in contact with them. The observed absence of chalcopyrite disease in sulfide ores metamorphosed to upper amphibolite and granulite facies (Lockington et al., 2014) may be ascribed to the production and isolation of Cu-rich partial melts under such conditions as the increased quantity of melt would promote its separation from the residual matrix minerals including chalcopyrite-diseased sphalerite.

IMPLICATIONS

Despite being a commonly observed feature in base metal sulfide deposits, chalcopyrite disease has eluded a convincing explanation till date. In the light of the growing acceptance of sulfide partial melting as an important ore genetic process, the finding in this study that metamorphism, culminating in sulfide partial melting, may promote formation of chalcopyrite disease textures has far reaching implications on identifying potential ore bodies, particularly those of valuable incompatible chalcophile elements. This is contrary to the fact that metamorphism generally tends to produce homogeneity and metamorphism-driven sulfide partial melting thus is the least-doubted mechanism behind the formation of chalcopyrite disease. As demonstrated in this study chalcopyrite disease is an indirect

consequence of partial melting, developed due to subsolidus diffusion of Cu, and is unlikely to be obliterated since it is itself a result of reequilibration. The mobility of Cu is forced by the nonstoichiometric high S in sphalerite together with the presence of an S-deficient Cu-enriched melt, produced during sulfide partial melting. Thus, chalcopyrite disease can be used as a potential evidence for melting in sulfide ores caused due to metamorphism.

ACKNOWLEDGEMENTS

BG thanks the CSIR, New Delhi for the financial assistance in the form of a Research Fellowship. The experimental work was performed using the facility supported by the project SR/S4/ES-219/2006 to KLP from the Department of Science and Technology (DST), New Delhi. SEM-BSE imaging and EPMA data were generated by the equipment procured through a DST funding (IR/S4/ESF-08/2005) to the Department of Geology and Geophysics, IIT Kharagpur. Critical reviews by Ron Frost and John Mavrogenes have substantially improved the quality of the paper. The authors thank Raúl Fonseca for the editorial handling.

REFERENCES

Barton, P.B., Jr. (1978) Some ore textures involving sphalente from the Furutobe mine, Akita Prefecture, Japan. Mining Geology, 28, 293–300.

Barton, P.B., Jr., and Bethke, P.M. (1987) Chalcopyrite disease in sphalerite:pathology and epidemiology. American Mineralogist, 72, 451–467.

Barton, P.B., Jr., and Skinner, B.J. (1967) Sulfide mineral stabilities. In H.L. Barnes, Ed., Geochemistry of Hydrothermal Ore Deposits. Holt, Rinehart and Winston, New York.

Bente, K., and Doering, T. (1993) Solid-state diffusion in sphalerites:an experimental verification of the "chalcopyrite disease". European Journal of Mineralogy, 5, 465–478.

Bente, K., and Doering, T. (1995) Experimental studies on the solid state diffusion of Cu + In in ZnS and on "Disease", DIS (Diffusion Induced Segregations), in sphalerite and their geological applications. Mineralogy and Petrology, 53, 285–305.

Bortnikov, N.S., Genkin, A.D., Dobrovol'skaya, M.G., Muravitskaya, G.N., and Filimonova, A.A. (1991) The nature of chalcopyrite inclusions in sphalerite: exsolution, coprecipitation, or "disease"? Economic Geology, 86, 1070-1082.

Chen, J., Chen, Y., and Li, Y. (2010) Effect of vacancy defects on electronic properties and activation of sphalerite (110) surface by first-principles. Transactions of Nonferrous Metals Society of China, 20, 502–506.

Eldridge, C.S., Bourcier, W.L., Ohmoto, H., and Barnes, H.L. (1988) Hydrothermal inoculation and incubation of the chalcopyrite disease in sphalerite. Economic Geology, 83, 978–989.

Frost, B.R., Mavrogenes, J.A., and Tomkins, A.G. (2002) Partial melting of sulfide ore deposits during medium- and high-grade metamorphism. Canadian Mineralogist, 40, 1–18.

Frost, B.R., Swapp, S.M., and Mavrogenes, J.A. (2011) Textural evidence for extensive melting of the Broken Hill ore body. Economic Geology, 106, 869–882.

Hutchison, M.N., and Scott, S.D. (1981) Sphalerite geobarometry in the system Cu-Fe-Zn-S. Economic Geology, 76, 143–153.

Jehan, N. (2015) Melting Experiment in the System PbS-ZnS-FeS-Cu_2S-S: Implications to Metamorphosed Massive Sulfide Deposits, 131 p. Ph.D. thesis, Indian Institute of Technology, Kharagpur, India.

Klekovkina, V.V., Gainov, R.R., Vagizov, F.G., Dooglav, A.V., Golovanecskiy, V.A., and Pen'kov, I.N. (2014) Oxidation and magnetic states of chalcopyrite $CuFeS_2$: a first principles calculation. Optics and Spectroscopy, 885–888, 116.

Kojima, S. (1990) A coprecipitation experiment on intimate association of sphalerite and chalcopyriteand its bearings on the genesis ofkuroko ores. Mining Geology, 40, 147-158.

Kojima, S., Nagase, T., and Inoue, T.A. (1995) Coprecipitation experiment on the chalcopyrite disease texture involving Fe-bearing sphalerite. Journal of Mineralogy, petrology and Economic Geology, 90, 261–267.

Kojima, S., and Sugaki, A. (1984) Phase relations in the central portion of the Cu-Fe-Zn-S system between 800 ° and 500 °C. Mineralogical Journal, 12, 15–28.

Kojima, S., and Sugaki, A. (1985) Phase relations in the Cu-Fe-Zn-S system between 500 ° and 300 °C under hydrothermal conditions. Economic Geology, 80, 158–171.

Kojima, S., and Sugaki, A. (1987) An Experimental Study on Chalcopyritization of SphaleriteInduced by Hydrothermally Metasomatic Reactions. Mining Geology, 36, no. 6, 373-380.

Lepetit, P., Bente, K., Doering, T., and Luckhaus, S. (2003) Crystal chemistry of Fe-containing sphalerites. Physics and Chemistry of Minerals, 30, 185–191.

Lockington, J.A., Cook, N.J., and Ciobanu, C.L. (2014) Trace and minor elements in sphalerite from metamorphosed sulphide deposits. Mineralogy and Petrology, 108, 873–890.

Mavrogenes, J.A., Frost, R., and Sparks, H.A. (2013) Experimental evidence of sulfide melt evolution via immiscibility and fractional crystallization. Canadian Mineralogist, 51, 841–850.

Mavrogenes, J.A., MacIntosh, W.I., and Ellis, D. (2001) Partial melting of the Broken Hill galena-sphalerite ore: experimental studies in the system PbS-FeS-ZnS-(Ag_2S). Economic Geology, 96, 205–210.

Mishra, B., and Bernhardt, H.-J. (2009) Metamorphism, graphite crystallinity and sulfide anatexis of the Rampura-Agucha massive sulfide deposit, northwestern India. Mineralium Deposita, 44, 183–204.

Morehead, F.F. (1963) A dember effect study of shifts in the stoichiometry of ZnS. Journal of The Electrochemical Society, 110, 285–288.

Pearce, C.I., Pattrick, R.A.D., Vaughan, D.J., Henderson, C.M.B., and van der Laan, G. (2006) Copper oxidation state in chalcopyrite: mixed Cu d^9 and d^{10} characteristics. Geochimica et Cosmochimica Acta, 70, 4635–4642.

Pruseth, K.L., Jehan, N., Sahu, P., and Mishra, B. (2014) The possibility of a ZnS-bearing sulfide melt at 600 °C: Evidence from the Rajpura–Dariba deposit, India, supported by laboratory melting experiment. Ore Geology Reviews, 60, 50–59.

Pruseth, K.L., Mishra, B., and Bernhardt, H.-J. (1997) Phase relations in the Cu_2S-PbS-Sb_2S_3 system: an experimental appraisal and application to natural polymetallic sulfide ores. Economic Geology, 92, 720–732.

Pruseth, K.L., Mishra, B., Jehan, N., and Kumar, B. (2016) Evidence of sulfide melting and melt fractionation during amphibolite facies metamorphism of the Rajpura-Dariba polymetallic sulfide ores. Ore Geology Reviews, 72, 1213–1223.

Pruseth, K.L., and Sahu, P. (2017) Pyrite nanoparticles: potential source of As in groundwater. Goldschmidt Conference, Paris.

Scott, S.D. (1974) Experimental methods in sulfide synthesis. In P.H. Ribbe, Ed., Sulfide Mineralogy, Reviews in Mineralogy, S1–S38. Mineralogical Society of America.

Scott, S.D. (1983) Chemical behavior of sphalerite and arsenopyrite in hydrothermal and metamorphic environments. Mineralogical Magazine, 47, 427–435.

Scott, S.D., and Barnes, H.L. (1971) Sphalerite geothermometry and geobarometry. Economic Geology, 66, 653–669.

Sharma, R.C., and Chang, Y.A. (1996) The S-Zn (sulfur-zinc) system. Journal of Phase Equilibria, 17, 261–266.

Sparks, H.A., and Mavrogenes, J.A. (2005) Sulfide melt inclusions as evidence for the existence of a sulfide partial melt at Broken Hill, Australia. Economic Geology, 100, 773–779.

Stevens, G., Prinz, S., and Rozendaal, A. (2005) Partial melting of the assemblage sphalerite + galena + pyrrhotite + chalcopyrite + sulfur: implications for high-grade metamorphosed massive sulfide deposits. Economic Geology, 100, 781–786.

Sugaki, A., Kitakaze, A., and Kojima, S. (1987) Bulk compositions of intimate intergrowths of chalcopyrite and sphalerite and their genetic implications. Mineralium Deposita, 22, 26–32.

453 Tomkins, A.G., and Mavrogenes, J.A. (2002) Mobilization of gold as a polymetallic melt
454 during pelite anatexis at the Challenger deposit, South Australia: a metamorphosed
455 Archean gold deposit. Economic Geology, 97, 1249–1271.

456 Tomkins, A.G., and Mavrogenes, J.A. (2003) Generation of metal-rich felsic magmas during
457 crustal anatexis. Geology, 31, 765–768.

458 Tomkins, A.G., Pattison, D.R.M., and Frost, B.R. (2007) On the initiation of metamorphic
459 sulfide anatexis. Journal of Petrology, 48, 511–535.

460 Wiggins, L.B., and Craig, J.R. (1980) Reconnaissance of the Cu-Fe-Zn-S system: Sphalerite
461 phase relationships. Economic Geology, 75, 742–751.

462

463

Figure Captions

FIGURE 1. Reflected light photomicrographs showing chalcopyrite disease in sphalerite from Rajpura-Dariba in Rajasthan, India. Probable grain-boundary and crystallographically controlled distribution of chalcopyrite blebs (A); localized coarsening of chalcopyrite blebs giving rise to intergrowth as observed in case of co-crystallization (B).

FIGURE 2. Run and melt compositions at 600 °C plotted in the ZnS-PbS-FeS-Cu_2S quaternary diagram (A) and ZnS-PbS-FeS-As_2S_3 quaternary diagram (B). The lengths of the sticks are proportional to the respective Cu_2S- and As_2S_3-contents. Filled circles represent the bulk run compositions and the unfilled circles represent the corresponding melt compositions.

FIGURE 3. SEM-BSE images showing stable phases and quenched melt textures from G19, G20, G18 and G21 at 600 °C (A, C, E and G respectively) and corresponding annealed textures at 350 °C (B, D, F and H, respectively). Sp = sphalerite; Gn = galena; Lo = löllingite; Iss = intermediate solid solution; Asp = arsenopyrite.

FIGURE 4. Plots showing the degree of nonstoichiometry in sphalerite (Sp; A), galena (Gn; B), intermediate solid solution (Iss; C) and melt (D) in the 600 °C (squares) and 350 °C (circles) experimental run products.

FIGURE 5. Photomicrograph of sphalerite grains showing chalcopyrite disease around undiseased cores (A) and concentrations profiles of Zn, Fe and Cu across a selected sphalerite grain (B) in the run product of G20 annealed at 350 °C.

FIGURE 6. BSE-image (A) and X-ray element maps of Cu, Fe, Zn and S (B–E) in a sphalerite grain in the run product of G20 annealed at 350 °C.

FIGURE 7. Plot showing the increase of S/(Fe+Zn) with increasing Fe-content of sphalerite.

This is a preprint, the final version is subject to change, of the American Mineralogist (MSA)
Cite as Authors (Year) Title. American Mineralogist, in press.
DOI: https://doi.org/10.2138/am-2018-6477

TABLE 1. Details of the run compositions and average EPMA analyses of different phases obtained at 600 °C in the run products along with their associated standard deviations (indicated in parentheses).

Run No.	Mol%					Duration (days)	At%						Formula						Phase (n)
	PbS	FeS	ZnS	Cu_2S	As_2S_3		**S**	**Fe**	**Cu**	**Zn**	**As**	**Pb**	**S**	**Fe**	**Cu**	**Zn**	**As**	**Pb**	
G18	14	50	27	5	5	10	50.36 (0.29)	32.10 (0.37)	12.22 (0.25)	5.18 (0.46)	0.14 (0.21)	bdl	3	1.91	0.73	0.31	0.01	0.00	Iss (10)
							50.38 (0.42)	0.78 (0.40)	0.30 (0.22)	0.71 (0.40)	0.06 (0.09)	47.77 (0.44)	1	0.02	0.01	0.01	0.00	0.95	Gn (11)
							50.86 (0.43)	16.24 (0.22)	0.91 (0.09)	31.99 (0.35)	bdl	bdl	1	0.32	0.02	0.63	0.00	0.00	Sp (9)
							41.55 (0.79)	22.06 (1.71)	3.99 (0.52)	0.85 (0.03)	24.53 (0.42)	7.02 (0.78)	1	0.53	0.10	0.02	0.59	0.17	Melt (5)
G19	10	16	64	5	5	10	49.82 (0.24)	0.19 (0.08)	0.57 (0.30)	1.78 (0.51)	0.09 (0.09)	47.54 (0.48)	1	0.00	0.01	0.04	0.00	0.95	Gn (6)
							50.32 (0.20)	7.37 (0.11)	0.28 (0.04)	42.03 (0.19)	bdl	bdl	1	0.15	0.01	0.84	0.00	0.00	Sp (9)
							5.92 (1.72)	33.11 (0.41)	0.56 (0.18)	1.52 (0.74)	58.89 (1.79)	bdl	0.18	1.00	0.02	0.05	1.78	0.00	Lo (11)
							44.99 (0.57)	3.53 (0.44)	24.87 (1.45)	3.30 (2.13)	9.66 (0.70)	13.65 (1.45)	1	0.08	0.55	0.07	0.21	0.30	Melt (6)
G20	50	14	27	5	5	10	50.87 0.33	0.07 0.08	0.29 0.19	0.49 0.40	0.02 0.03	48.27 0.38	1	0.00	0.01	0.01	0.00	0.95	Gn (7)
							50.37 (0.20)	10.98 (0.13)	0.55 (0.08)	38.10 (0.22)	bdl	bdl	1	0.22	0.01	0.76	0.00	0.00	Sp (8)
							30.76 (0.84)	31.84 (0.90)	1.69 (0.50)	0.30 (0.16)	34.69 (0.94)	0.73 (0.54)	1	1.03	0.05	0.01	1.13	0.02	Asp (10)
							47.58 (0.62)	3.69 (0.65)	21.89 (1.52)	0.48 (0.23)	11.77 (1.42)	14.59 (1.52)	1	0.08	0.46	0.01	0.25	0.31	Melt (10)
G21	23	5	63	5	5	10	47.95 (0.56)	0.17 (0.18)	3.16 (0.30)	4.27 (1.25)	0.09 (0.04)	44.36 (0.72)	1	0.00	0.07	0.09	0.00	0.92	Gn (12)
							50.21 (0.11)	0.62 (0.51)	0.34 (0.10)	48.80 (0.58)	bdl	bdl	1	0.01	0.01	0.97	0.00	0.00	Sp (10)
							0.29 (0.38)	32.90 (0.82)	0.49 (0.32)	1.63 (0.79)	64.65 (0.70)	0.05 (0.07)	0.01	1.02	0.02	0.05	2.00	0.00	Lo (14)

This is a preprint, the final version is subject to change, of the American Mineralogist (MSA)
Cite as Authors (Year) Title. American Mineralogist, in press.
DOI: https://doi.org/10.2138/am-2018-6477

							2.64 (1.49)	0.06 (0.05)	65.75 (2.36)	1.41 (1.00)	30.12 (2.19)	bdl	0.09	0.00	2.18	0.05	1	0.00	Kt (6)
							37.51 (0.40)	1.44 (0.28)	47.31 (1.17)	1.20 (0.25)	1.27 (1.55)	11.28 (1.15)	1	0.04	1.26	0.03	0.03	0.30	Melt (4)
G22	40	38	12	5	5	10	50.51 (0.34)	31.94 (0.60)	12.67 (0.52)	4.86 (0.11)	0.02 (0.05)	bdl	3	1.90	0.75	0.29	0.00	0.00	Iss (18)
							50.67 (0.49)	0.64 (0.47)	0.28 (0.28)	0.3 (0.04)	0.03 (0.04)	48.08 (0.44)	1	0.01	0.01	0.01	0.00	0.95	Gn (13)
							51.10 (0.37)	16.14 (0.41)	0.85 (0.06)	31.90 (0.28)	bdl	bdl	1	0.32	0.02	0.62	0.00	0.00	Sp (12)
							53.05 (0.24)	45.64 (0.25)	1.25 (0.07)	0.06 (0.04)	bdl	bdl	1	0.86	0.02	0.00	0.00	0.00	Po (10)
							42.14 (0.94)	21.21 (1.73)	3.33 (0.44)	0.33 (0.08)	25.50 (0.70)	7.51 (0.85)	1	0.50	0.08	0.01	0.61	0.18	Melt (5)

*(n) is the number of analyses and 'bdl' stands for below detection limit. Melt compositions were determined by averaging several analyses obtained using a defocussed beam of 20 µm in diameter. Sp = sphalerite; Gn = galena; Iss = intermediate solid solution; Po = pyrrhotite; Asp = arsenopyrite; Lo = löllingite; Kt = koutekite.

486

487

TABLE 2. Average EPMA analyses and their standard deviations (provided in parentheses) of phases obtained after annealing at350 °C the run products of the experiments conducted at 600 °C.

Run No.	At%						Formula						Phase (n)
	S	Fe	Cu	Zn	As	Pb	S	Fe	Cu	Zn	As	Pb	
G18	50.17 (0.35)	29.92 (0.39)	14.86 (0.26)	4.98 (0.58)	0.07 (0.14)	bdl	3	1.79	0.89	0.30	0.00	0.00	Iss (12)
	49.96 (0.30)	0.85 (0.13)	0.30 (0.14)	0.83 (0.35)	0.06 (0.04)	48.00 (0.33)	1	0.02	0.01	0.02	0.00	0.96	Gn (9)
	50.46 (0.43)	16.33 (0.09)	1.06 (0.19)	32.15 (0.35)	bdl	bdl	1	0.32	0.02	0.64	0.00	0.00	Sp (6)
	34.38	32.55	1.24	0.74	30.93	0.16	1	0.95	0.04	0.02	0.90	0.00	Asp (10)

	(1.83)	(0.73)	(0.69)	(0.37)	(2.22)	(0.29)							
G19	49.90	0.15	0.40	1.84	0.02	47.70	1	0.00	0.01	0.04	0.00	0.96	Gn (6)
	(0.49)	(0.15)	(0.37)	(0.41)	(0.02)	(0.58)							
	50.45	7.26	0.63	41.64	bdl	bdl	1	0.14	0.01	0.83	0.00	0.00	Sp (15)
	(0.27)	(0.38)	(0.39)	(0.30)									
	6.25	33.02	0.57	1.53	58.54	0.09	0.19	1	0.02	0.05	1.77	0.00	Lo (10)
	(0.96)	(0.50)	(0.22)	(0.52)	(0.81)	(0.15)							
	45.97	4.28	23.92	2.83	9.24	13.75	1	0.09	0.52	0.06	0.20	0.30	Melt (6)§
	(0.27)	(0.40)	(1.07)	(1.02)	(0.53)	(1.06)							
G20	50.44	0.05	0.71	0.57	0.02	48.21	1	0.00	0.01	0.01	0.00	0.96	Gn (7)
	(0.54)	(0.06)	(0.26)	(0.35)	(0.02)	(0.56)							
	50.26	11.25	0.56	37.93	bdl	bdl	1	0.22	0.01	0.75	0.00	0.00	Sp (26)
	(0.32)	(0.11)	(0.1)	(0.33)									
	31.59	30.48	2.57	0.79	34.31	0.26	1	0.96	0.08	0.03	1.09	0.01	Asp (6)
	(2.04)	(1.10)	(1.62)	(0.32)	(2.57)	(0.33)							
	46.57	5.19	19.53	0.71	10.26	17.74	1	0.11	0.42	0.02	0.22	0.38	Melt (9) §
	(1.16)	(0.82)	(2.08)	(0.34)	(0.62)	(1.48)							
G21	47.92	0.27	3.74	2.98	0.08	45.01	1	0.01	0.08	0.06	0.00	0.94	Gn (11)
	(0.23)	(0.35)	(0.50)	(0.96)	(0.04)	(0.42)							
	50.39	0.39	1.02	48.19	bdl	bdl	1	0.01	0.02	0.96	0.00	0.00	Sp (14)
	(0.34)	(0.09)	(1.26)	(1.01)									
	0.16	33.13	0.46	1.70	64.53	0.02	0.00	1.03	0.01	0.05	2	0.00	Lo (14)
	(0.10)	(0.72)	(0.22)	(0.87)	(0.55)	(0.02)							
	0.49	0.07	69.28	0.97	29.18	0.01	0.02	0.00	2.37	0.03	1	0.00	Kt (6)
	(0.46)	(0.06)	(2.51)	(0.64)	(2.11)	(0.01)							
	30.79	0.54	67.31	0.65	0.31	0.47	1	0.02	2.19	0.02	0.01	0.02	Cc (9)
	(0.60)	(0.41)	(0.59)	(0.44)	(0.15)	(0.11)							
G22	50.15	29.96	14.59	4.60	0.65	0.05	3	1.79	0.87	0.28	0.04	0.00	Iss (9)
	(0.55)	(0.32)	(0.57)	(0.37)	(1.35)	(0.13)							
	50.19	0.75	0.37	0.33	0.03	48.34	1	0.01	0.01	0.01	0.00	0.96	Gn (6)
	(0.74)	(0.65)	(0.42)	(0.33)	(0.04)	(0.54)							
	50.94	15.88	1.19	31.99	bdl	bdl	1	0.31	0.02	0.63	0.00	0.00	Sp (4)
	(0.33)	(0.32)	(0.37)	(0.17)									

This is a preprint, the final version is subject to change, of the American Mineralogist (MSA)
Cite as Authors (Year) Title. American Mineralogist, in press.
DOI: https://doi.org/10.2138/am-2018-6477

53.26	46.52	0.21	0.01	0.01	bdl	1	0.87	0.00	0.00	0.00	0.00	Po (4)
(0.36)	(0.32)	(0.04)	(0.01)	(0.01)								
34.41	31.38	0.80	0.32	31.97	1.12	1	0.91	0.02	0.01	0.93	0.03	Asp (4)
(0.67)	(0.35)	(0.04)	(0.16)	(0.65)	(0.48)							

§ Annealed quenched melts. "bdl" stands for below detection limit and (n) is the number of analyses.

488

TABLE 3. EPMA analyses of a diseased sphalerite grain along the profile shown in Figure 5B.

Analysis no.	1	2	3	4	5	6	7	8	9	10	11
Wt%											
S	35.67	35.27	35.10	34.26	34.21	34.35	34.12	33.86	33.67	33.93	33.00
Fe	7.95	7.75	8.13	10.21	13.26	13.27	13.29	13.19	13.08	10.99	7.84
Cu	7.66	6.96	6.93	4.31	0.73	0.67	0.72	0.79	0.66	3.06	6.93
Zn	49.24	50.81	50.92	51.10	51.05	51.68	52.00	51.89	51.83	51.35	50.57
As	0.03	bdl	bdl	0.08	bdl	bdl	bdl	bdl	bdl	0.02	0.61
Pb	bdl	bdl	bdl	bdl	bdl	bdl	bdl	bdl	bdl	bdl	bdl
Total	100.5	100.8	101.1	99.9	99.3	100.0	100.1	99.7	99.2	99.3	99.0
Mol%											
FeS	14.01	13.54	14.09	17.71	23.06	22.88	22.78	22.66	22.58	19.10	13.73
CuS	11.87	10.68	10.55	6.57	1.12	1.02	1.09	1.20	1.00	4.67	10.66
ZnS	74.13	75.78	75.36	75.72	75.82	76.10	76.13	76.14	76.42	76.23	75.61

489

Figure 1

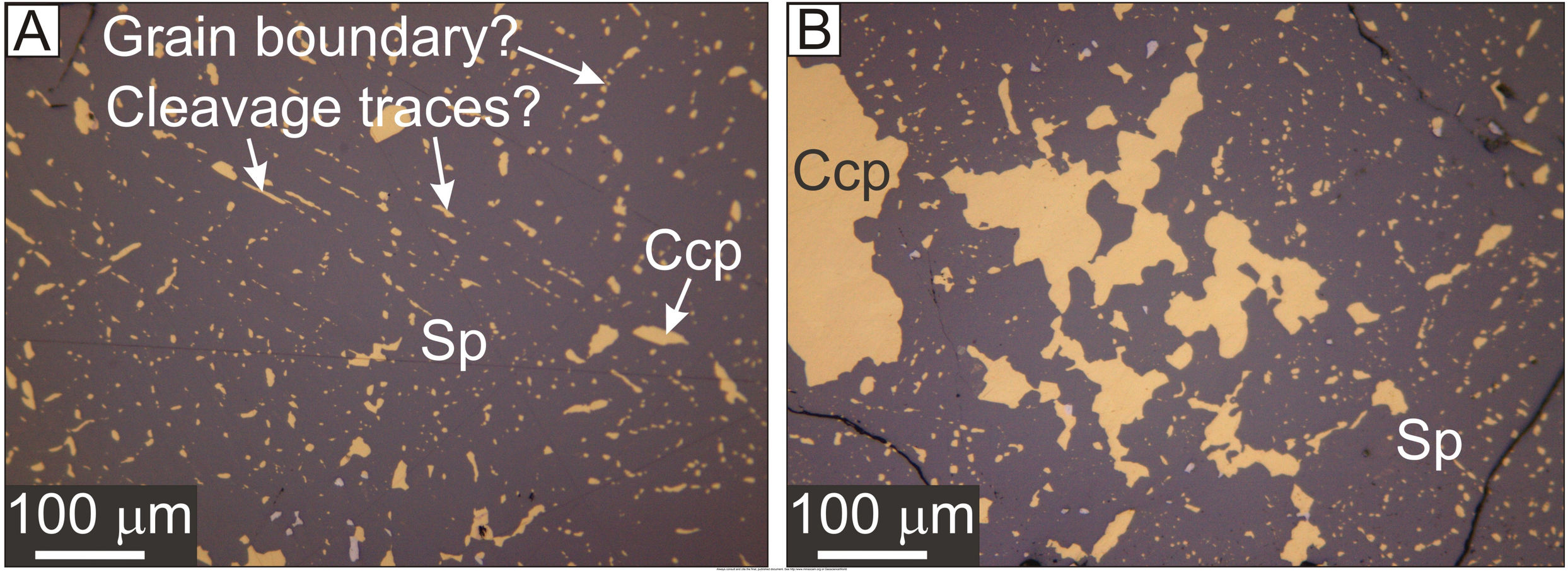

This is a preprint, the final version is subject to change, of the American Mineralogist (MSA)
Cite as Authors (Year) Title. American Mineralogist, in press.
DOI: https://doi.org/10.2138/am-2018-6477

Figure 2

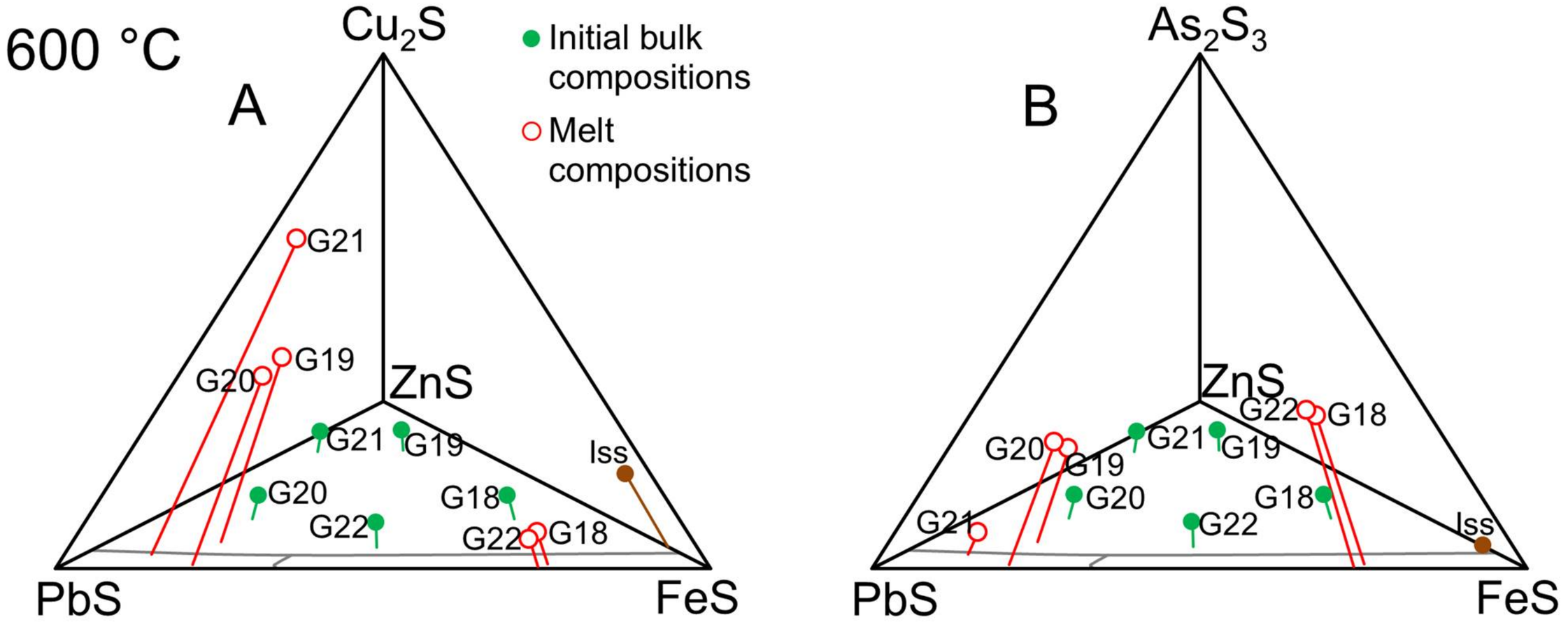

Figure 3

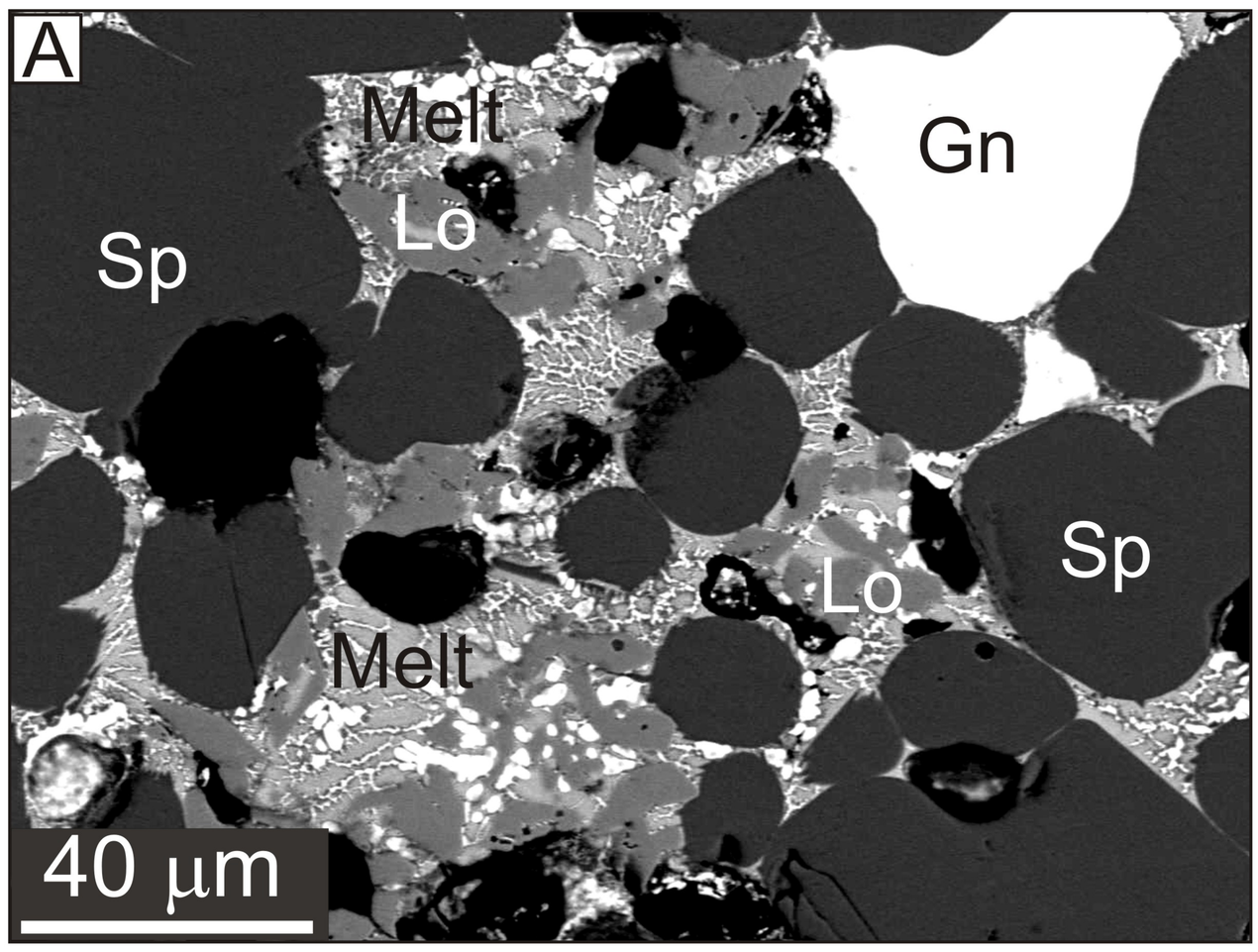

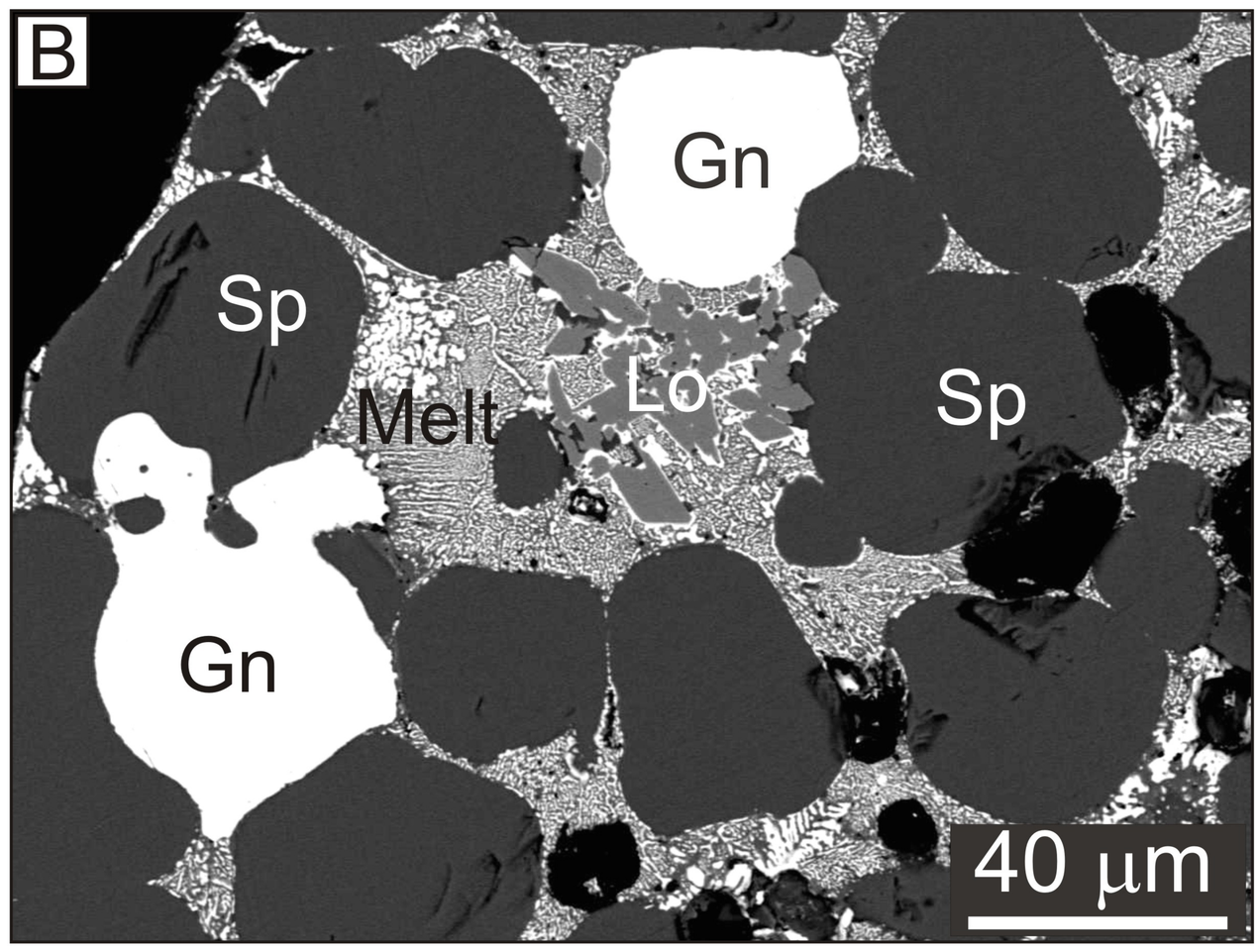

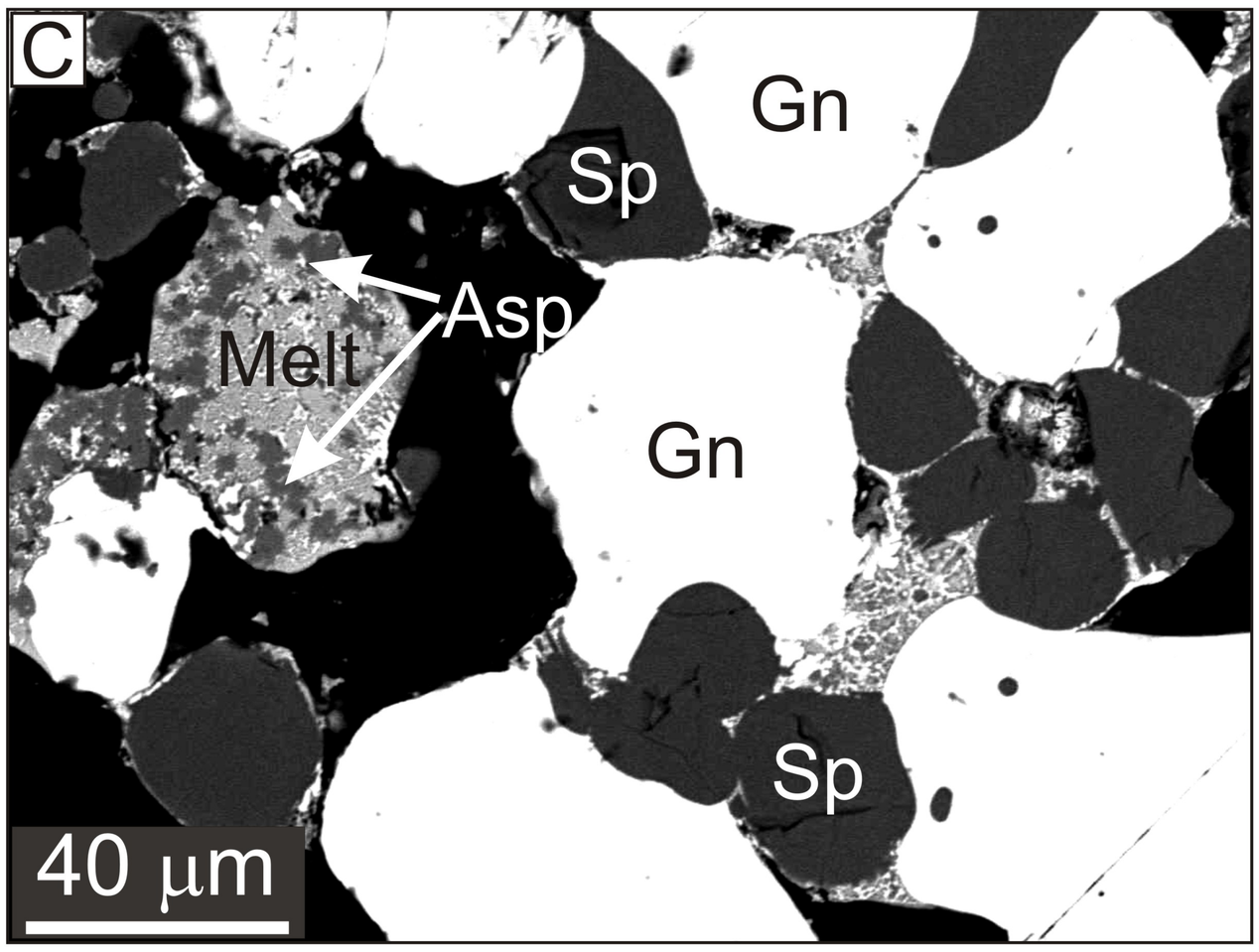

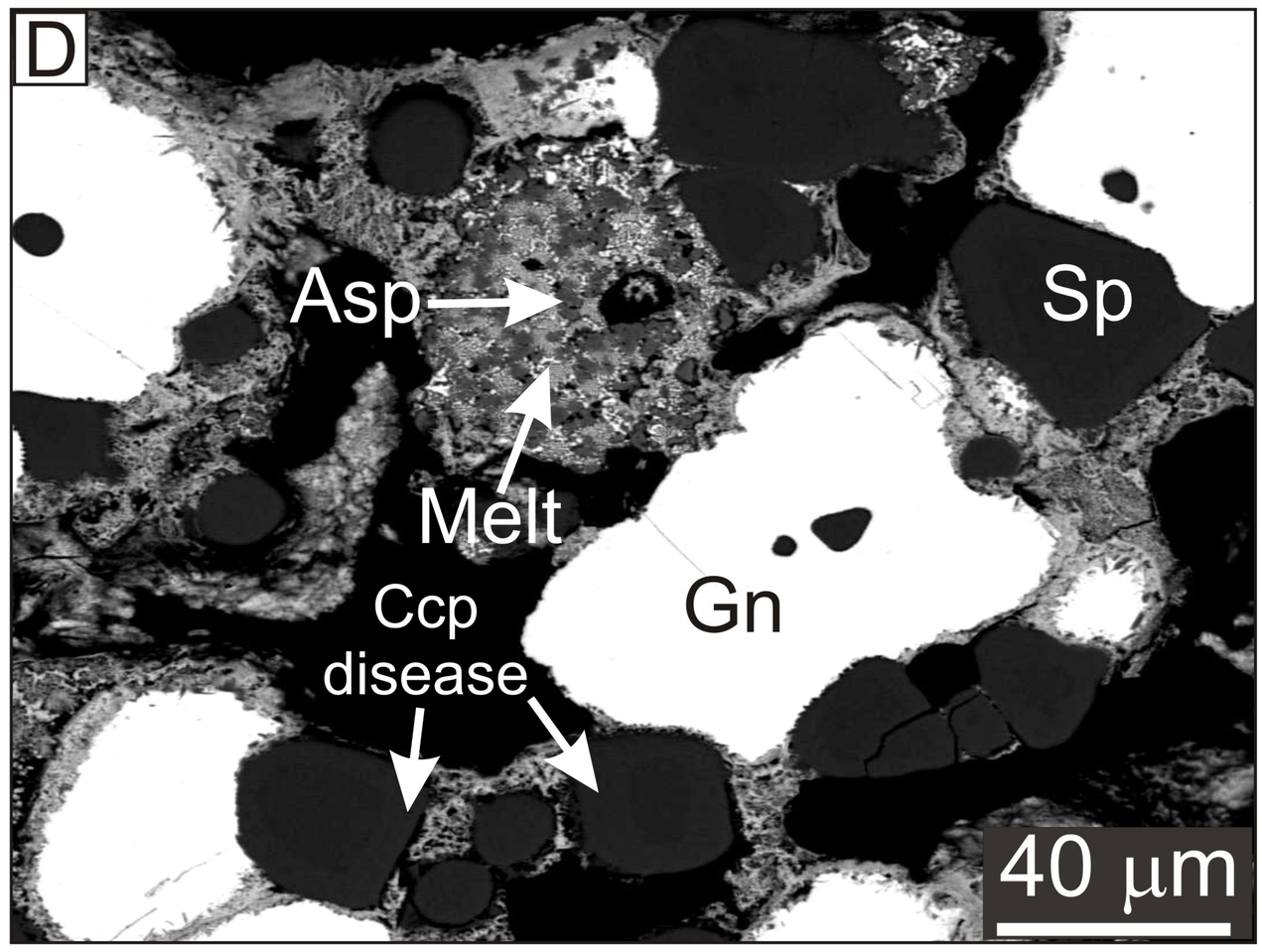

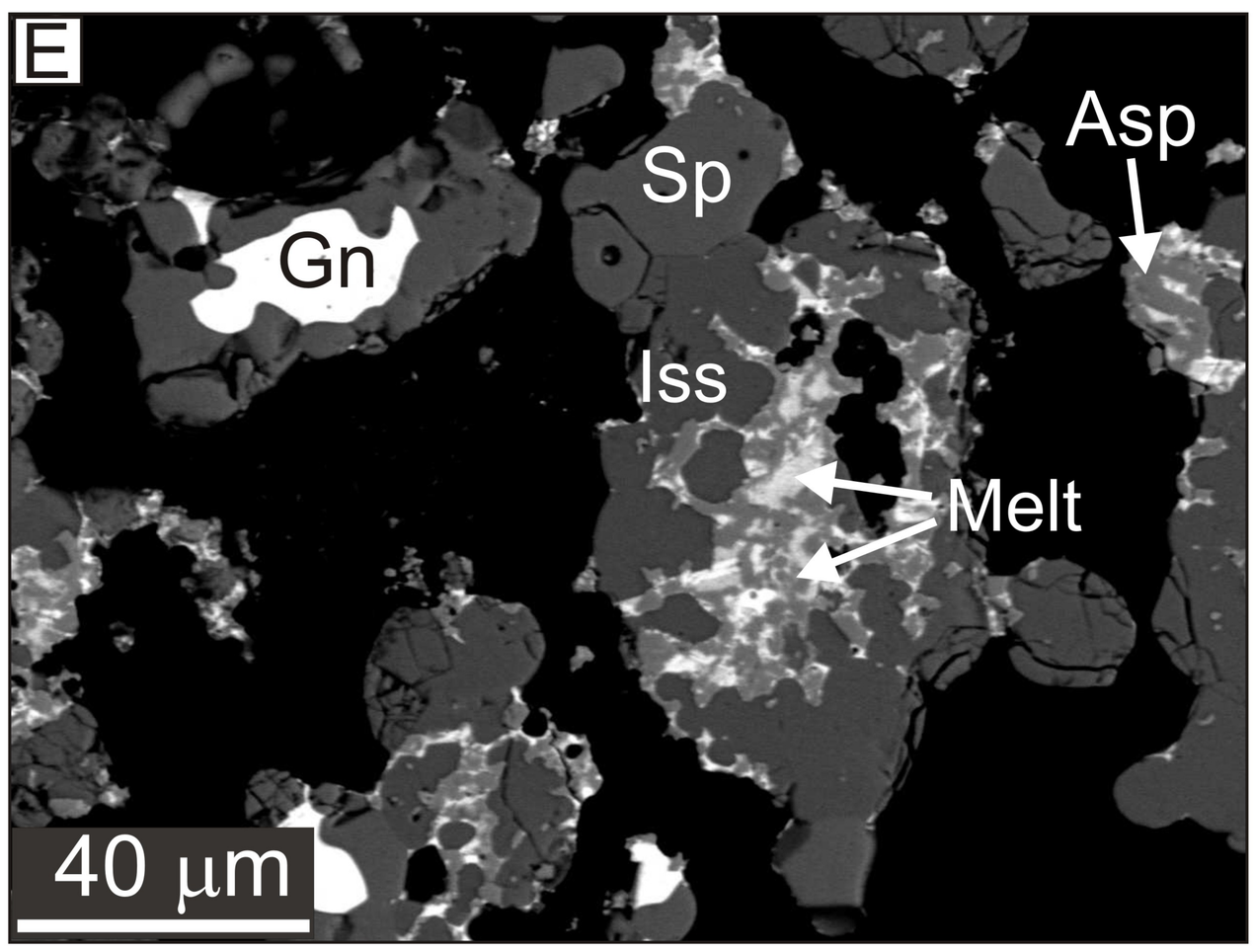

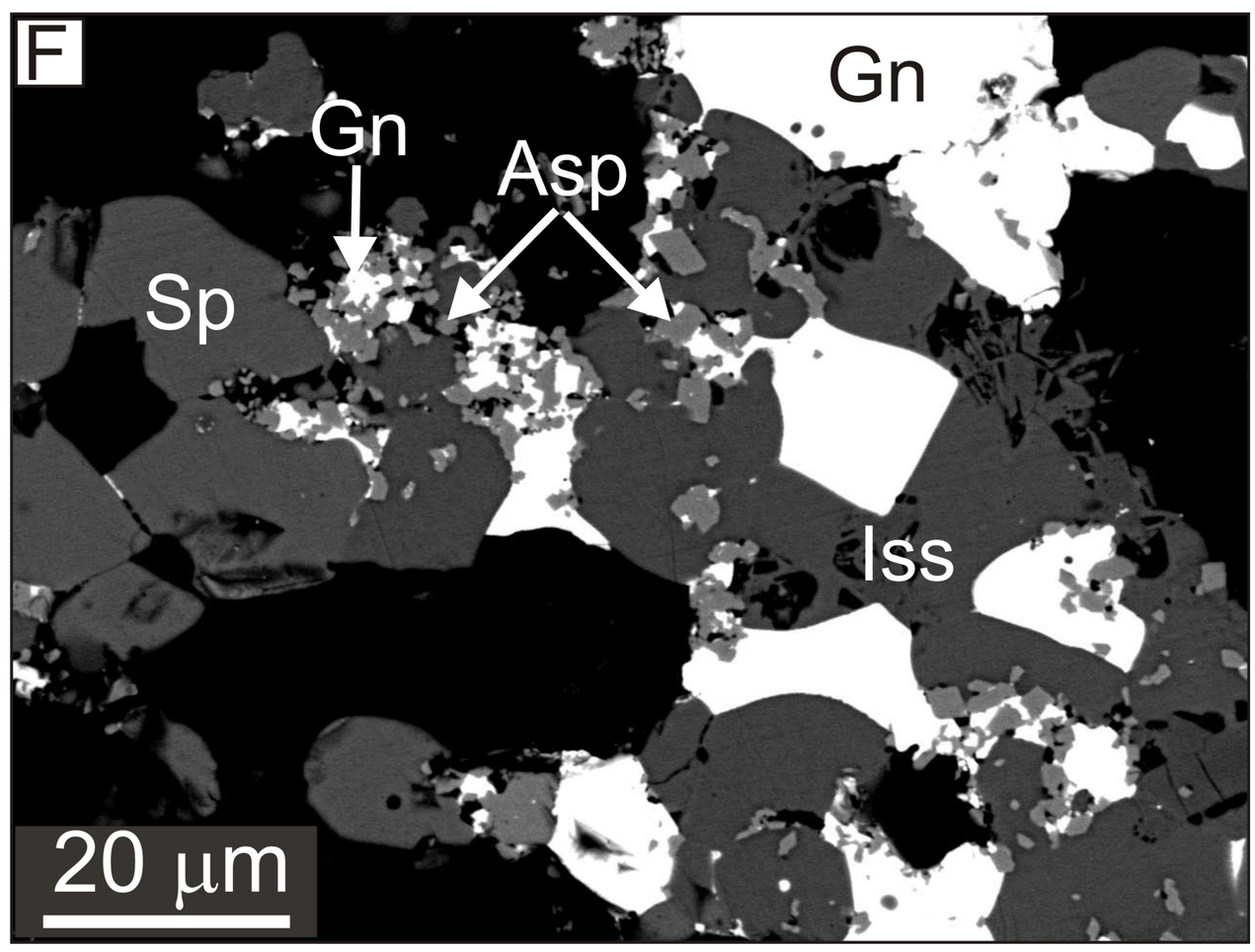

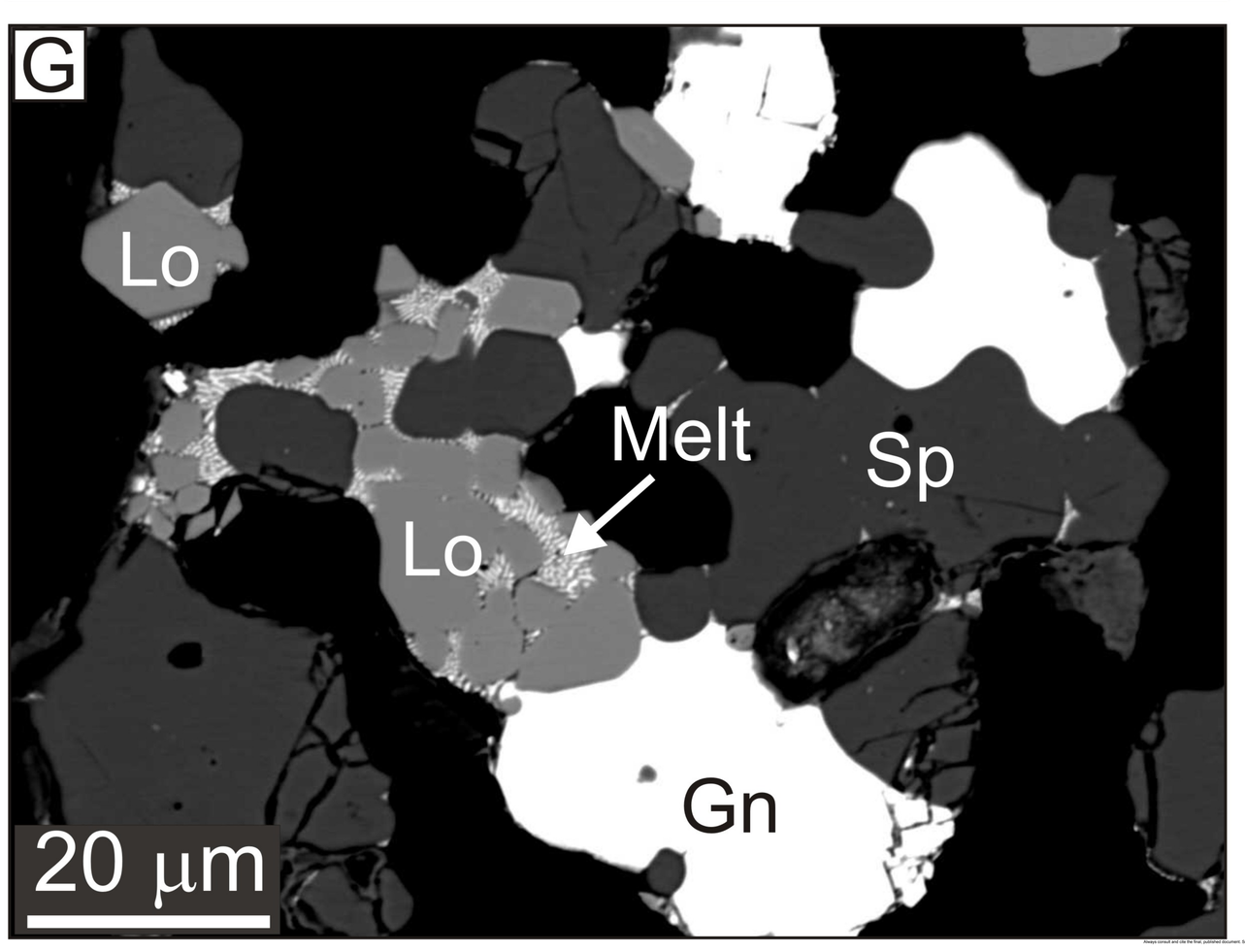

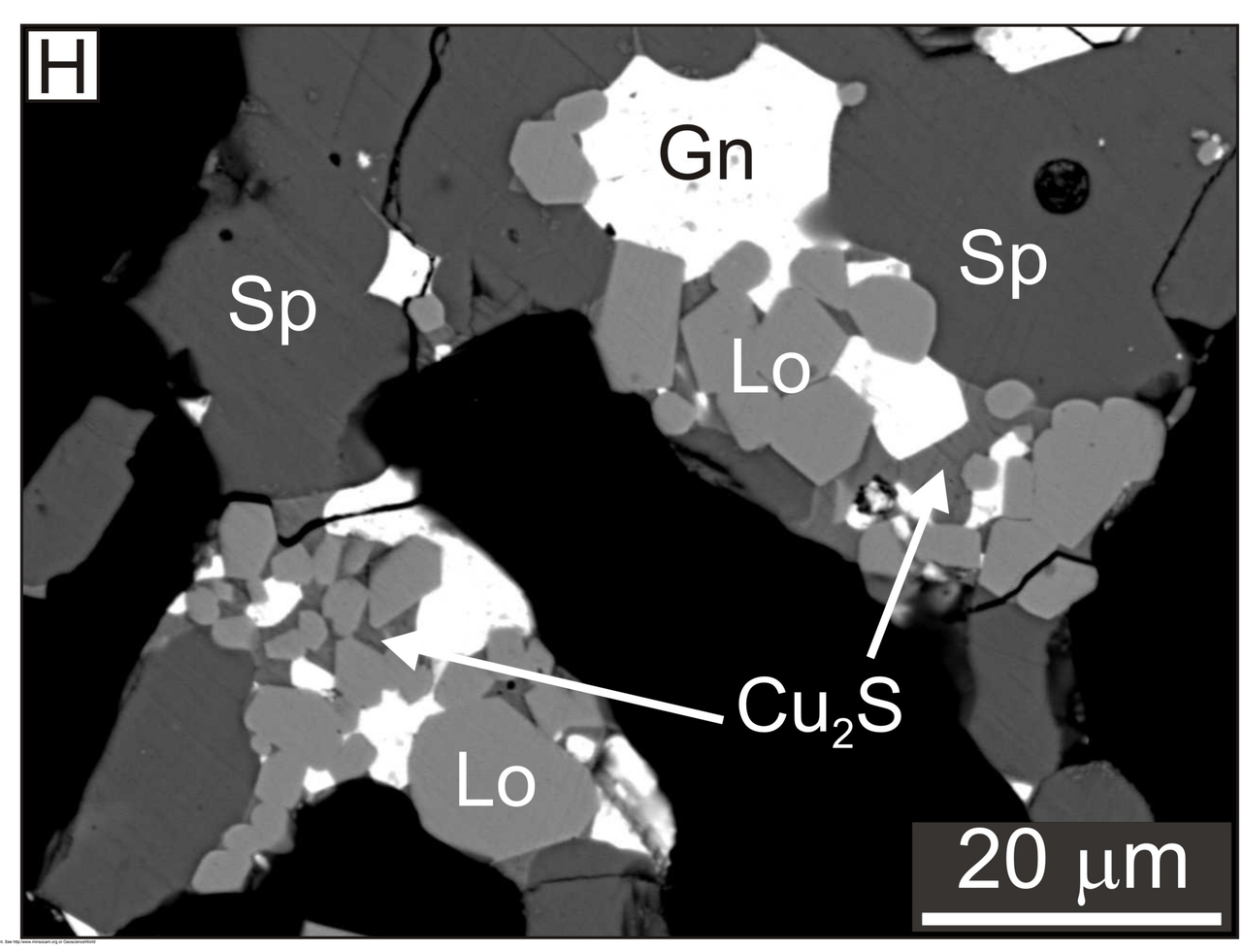

Figure 4

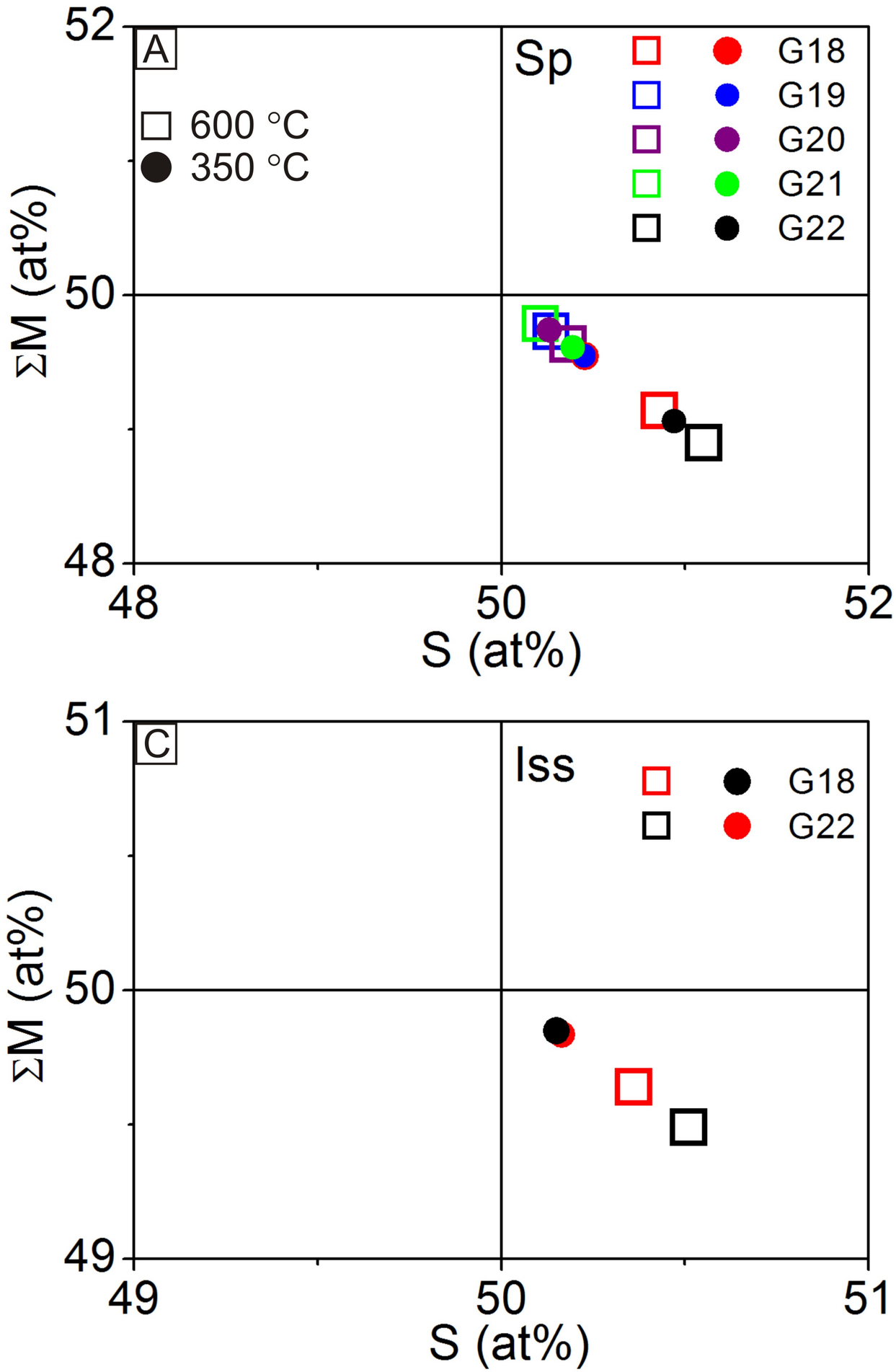

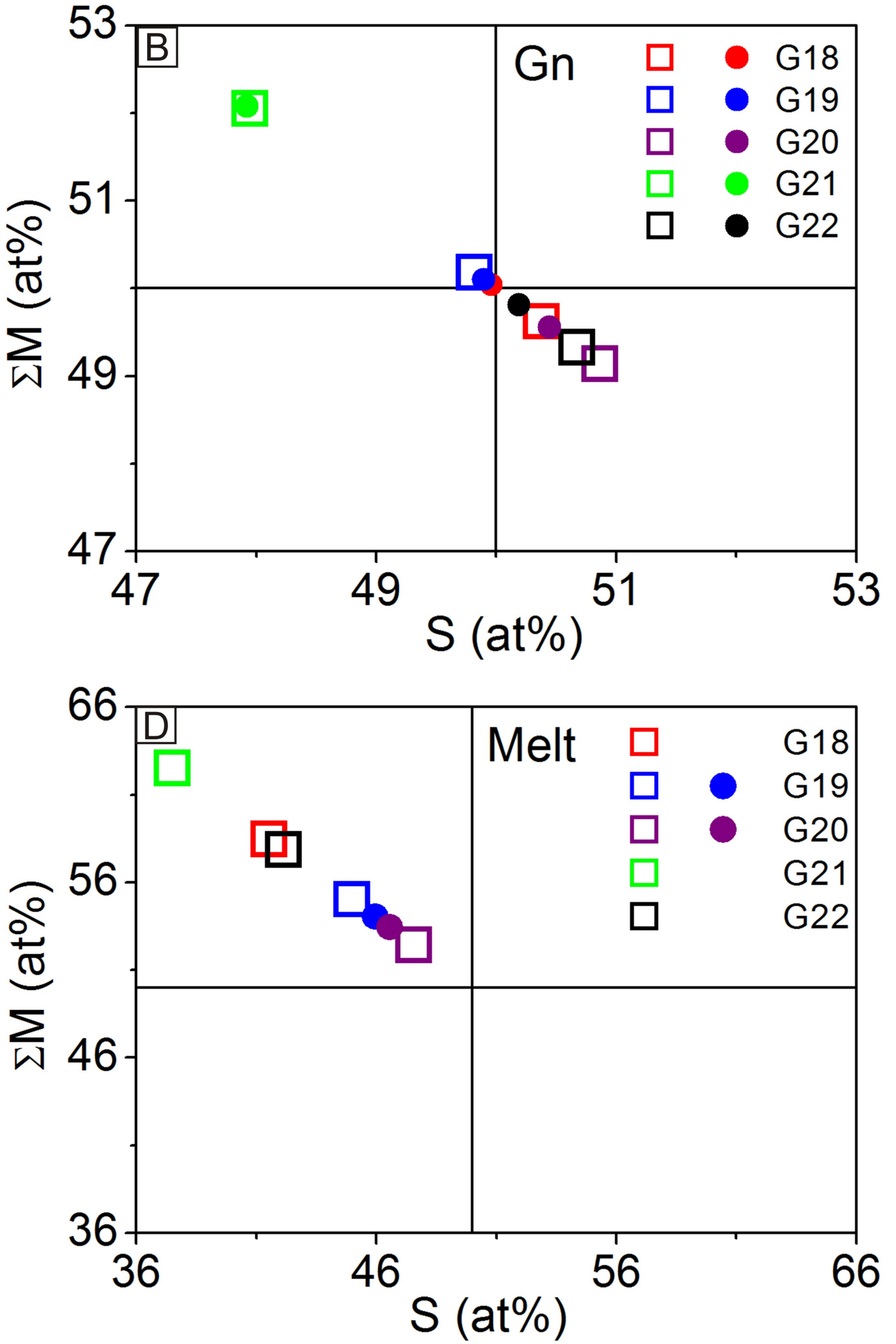

Figure 5

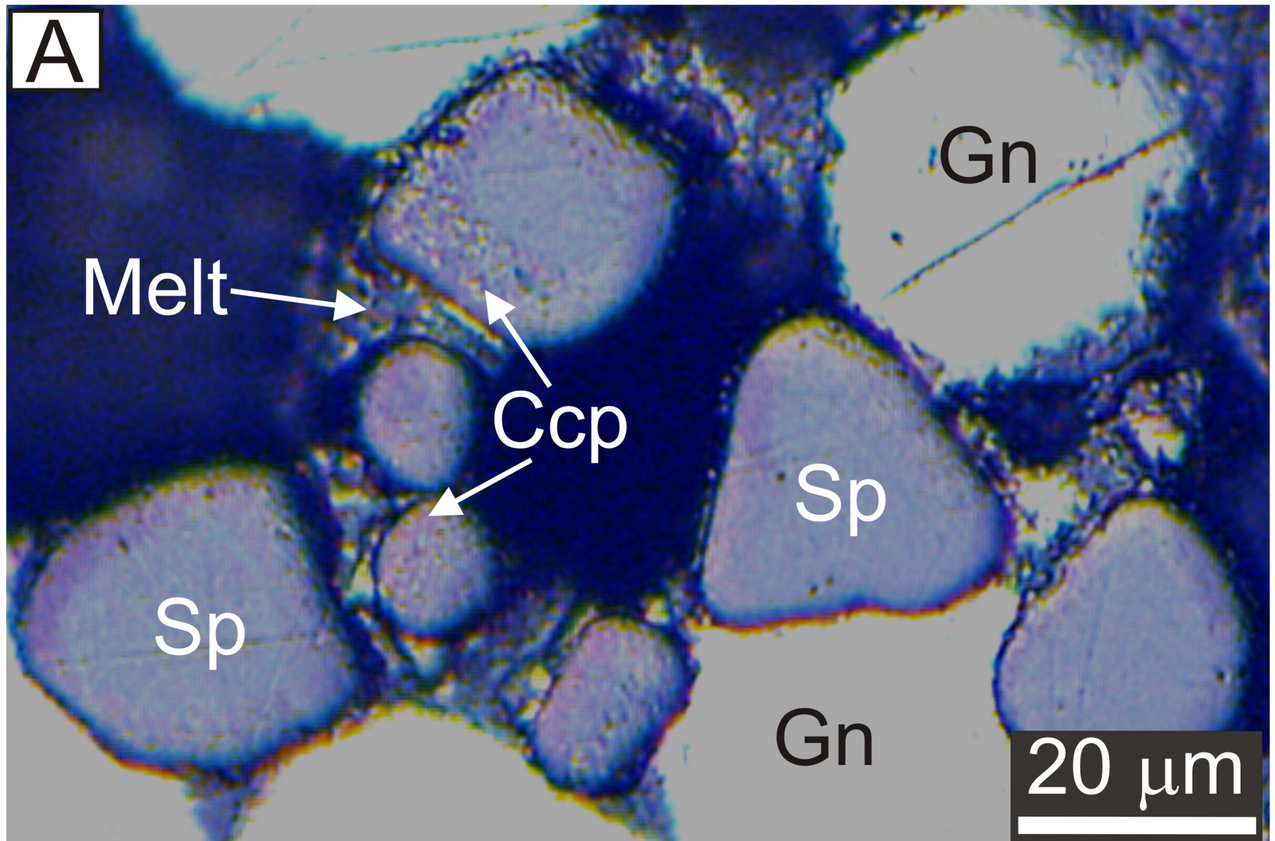

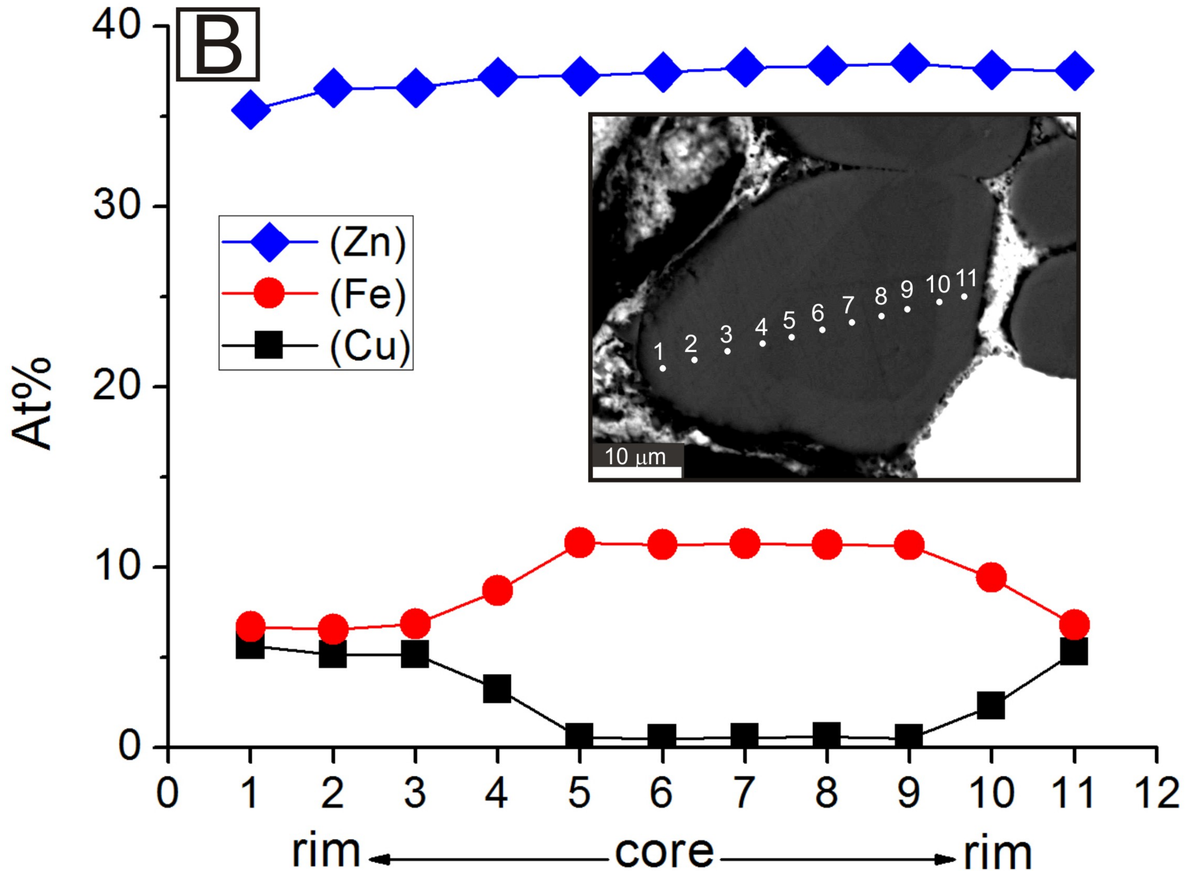

Figure 6

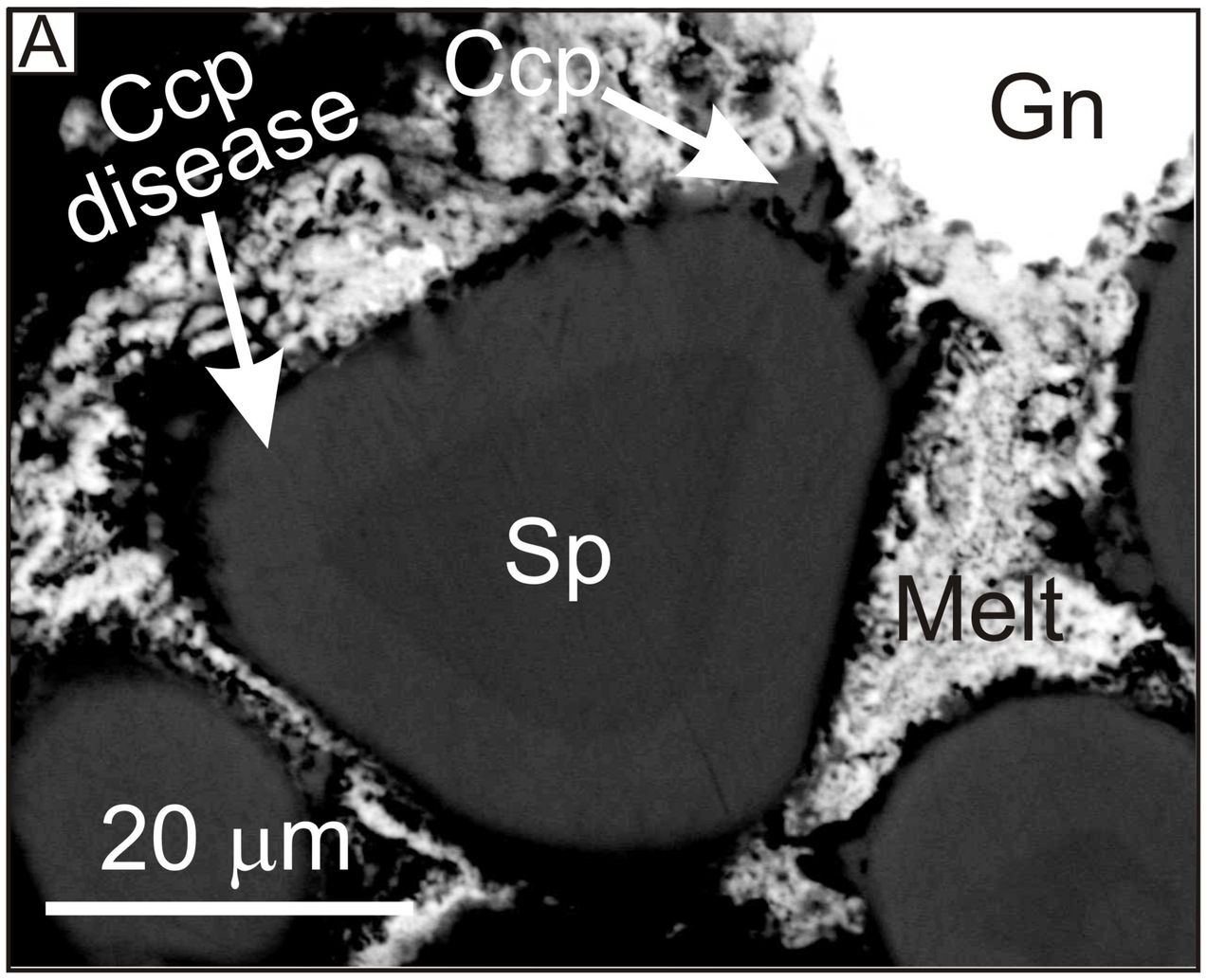

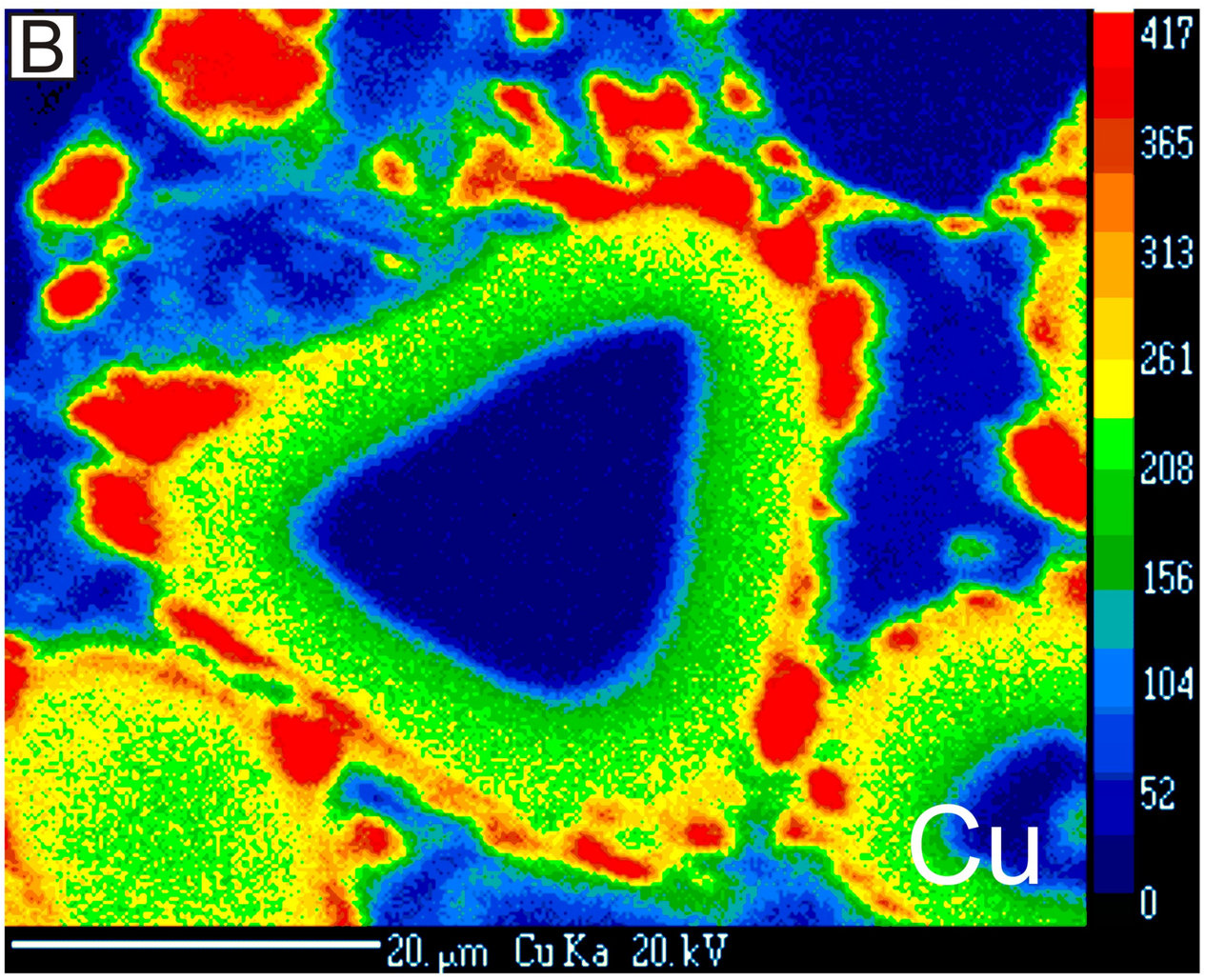

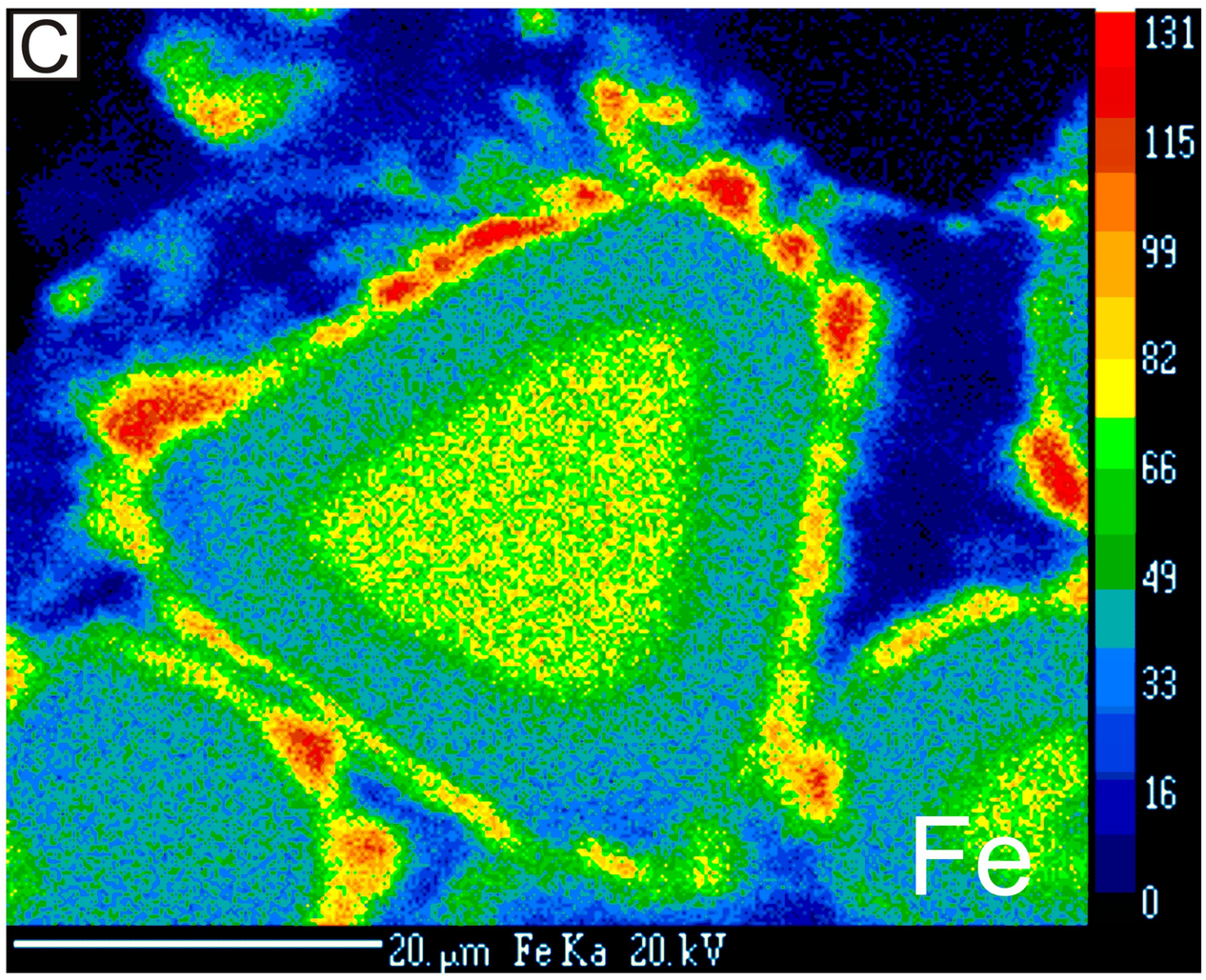

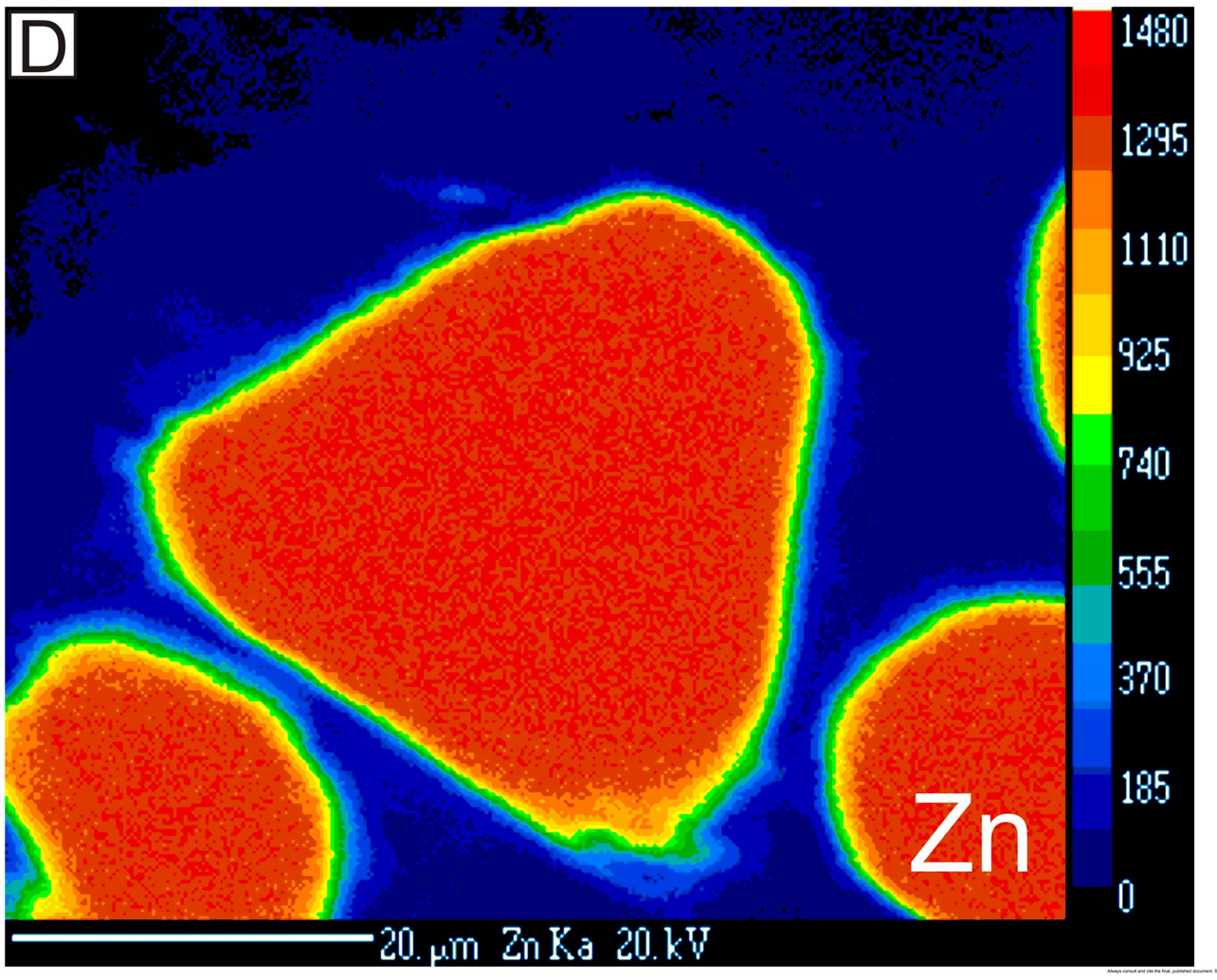

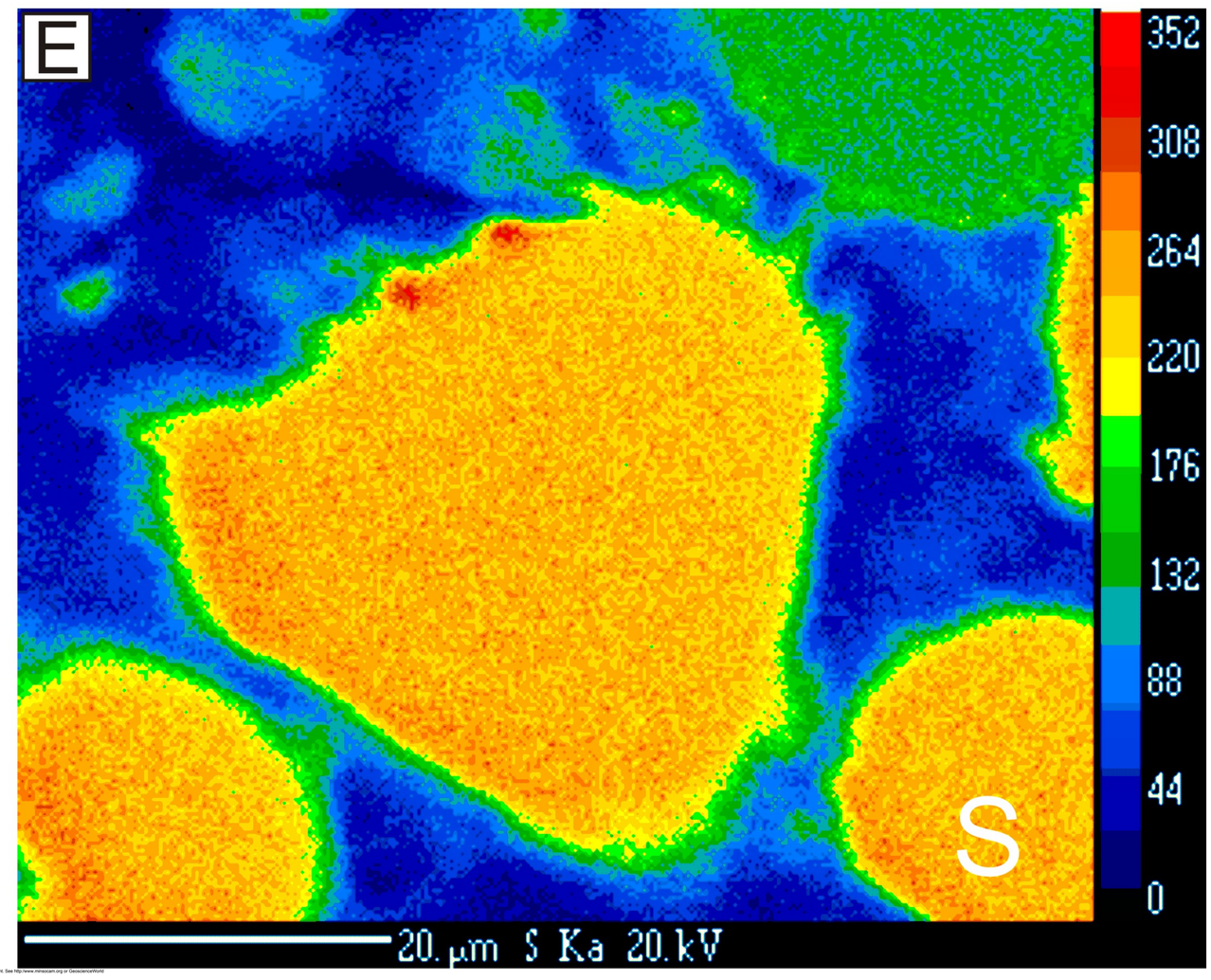

This is a preprint, the final version is subject to change, of the American Mineralogist (MSA)
Cite as Authors (Year) Title. American Mineralogist, in press.
DOI: https://doi.org/10.2138/am-2018-6477

Figure 7